FINAL REPORT

NASA GRANT NO. NSG–3106

INVESTIGATIONS OF LUBRICANT RHEOLOGY AS APPLIED TO ELASTOHYDRODYNAMIC LUBRICATION

Co–Principal Investigators:
S. Bair, Research Engineer
W. O. Winer, Professor

Prepared for

NASA–Lewis Research Center
21000 Brookpark Road
Cleveland, Ohio 44135

July, 1978

GEORGIA INSTITUTE OF TECHNOLOGY
SCHOOL OF MECHANICAL ENGINEERING
ATLANTA, GEORGIA 30332

1978

GEORGIA INSTITUTE OF TECHNOLOGY
School of Mechanical Engineering
Atlanta, Georgia 30332

INVESTIGATIONS OF LUBRICANT RHEOLOGY AS APPLIED TO ELASTOHYDRODYNAMIC LUBRICATION

Ward O. Winer, Ph.D
Professor
Principal Investigator

Scott Bair
Research Engineer
Principal Investigator

July, 1978

GEORGIA INSTITUTE OF TECHNOLOGY
SCHOOL OF MECHANICAL ENGINEERING
Atlanta, Georgia 30332

INVESTIGATIONS OF LUBRICANT RHEOLOGY AS APPLIED TO ELASTOHYDRODYNAMIC LUBRICATION

NASA GRANT NO.
NSG-3106

Co-Principal Investigators

S. Bair
Research Engineer

W. O. Winer
Professor

for

NASA-Lewis Research Center
21000 Brookpark Road
Cleveland, Ohio 44135

July, 1978

ABSTRACT

Measurements of lubricant shear rheological behavior in the amorphous solid region and near the liquid-solid transition are reported. Elastic, plastic and viscous behavior was observed. The maximum yield shear stress (limiting shear stress) is a function of temperature and pressure and is believed to be the property which determines the maximum traction in elastohydrodynamic contacts such as traction drives.

A shear rheological model based on primary laboratory data is proposed for concentrated contact lubrication. The model is a Maxwell model modified with a limiting shear stress. Three material properties are required: low shear stress viscosity, limiting elastic shear modulus, and the limiting shear stress the material can withstand. All three are functions of temperature and pressure. In applying the model to EHD contacts the predicted response possesses the characteristics expected from several experiments reported in the literature.

TABLE OF CONTENTS

LIST OF TABLES

LIST OF ILLUSTRATIONS

Figure

Figure

Figure

I. INTRODUCTION

In a previous contract report and publications [1,2] the authors have shown that, even based on low rate dilatometry experiments, many lubricants in typical elastohydrodynamic (EHD) contacts will be in a non-equilibrium amorphous solid state. The rate of environmental change experienced by a lubricant in an EHD contact is greater than that in the dilatometry experiment and, therefore, will increase the pressure-temperature region where amorphous solid behavior is to be expected. Nevertheless, the low rate dilatometry transitions are in good agreement with transition in traction behavior measured in the novel EHD experiments of Johnson et al. [3]. These are shown in Figure 1.

If lubricants undergo liquid-solid transitions in EHD contacts and behave in some cases as amorphous solids, their large strain, shear stress-shear strain behavior in the amorphous state should be examined. An average particle in a typical EHD contact undergoes large strain ($\geq$ 10%). Therefore behavior in small strain oscillatory experiments may not be relevant to EHD. Experiments were conducted to measure the shear stress-shear strain behavior of liquid lubricants under pressure in the amorphous solid state.

This report presents the measurements of the shear stress-strain behavior of lubricants in the amorphous solid region and near the liquid-solid transition determined by dilatometry. It is demonstrated that typical lubricants exhibit viscous, elastic, and plastic behavior in shear and that they have a limiting shear stress for

large strain. At a given pressure the limiting shear stress can be reached by lowering the temperature or increasing the shear rate. This limiting shear stress is the material property which determines the maximum shear stress that can be transmitted in an EHD contact and therefore in a traction drive device.

Elastic shear modulus and maximum elastic strain have also been measured and are reported. The techniques employed also permit the determination of the limiting low shear viscosity at very high levels of viscosity which agree well with traditional falling body viscosity measurements.

Speculation about a limiting shear strength of lubricant films has been made for many years. The fact that traction in EHD contacts seldom exceeds one tenth of the average pressure, and that this could not be explained in terms of a Newtonian viscous fluid with pressure dependent viscosity, led Smith (1959) [4] to propose a limiting shear stress for the lubricant. That is, it behaves as a plastic solid. The EHD experiments of Plint (1964) [5] and Johnson et al. [3, 6 and 7] support this view under some operating conditions.

The shear rheological response of lubricants in highly loaded contacts has been a vexing problem confronting the community for many years and has been the subject of much research and speculation. The environmental conditions to which the lubricant is subjected are apparently unique and very severe. It is essentially impossible to reproduce those conditions in primary laboratory measurements and consequently to date, concentrated contact traction has not been

predictable from primary laboratory measurements. This report presents a simple rheological model of lubricant behavior employing the primary property measurements also reported and an example of how the model can be used to predict EHD traction.

Johnson and Roberts [6] discuss the difficulty of distinguishing between different models from EHD data. This is particularly true in the low slide-roll ratio portion of the traction curve where small strains occur which could be either a viscous or elastic solid response. However, in their novel EHD experiments with controlled amounts of side slip and/or spin they convincingly demonstrate a viscous-solid transition and the inapplicability of the compressional visco-elasticity model.

Many different rheological models have been proposed but, apparently without exception, to predict contact behavior requires measurement of contact behavior and an adjustment of curve fitting material parameters. The discovery of the underlying physical properties seems to have escaped us to date. To be useful and readily accepted the primary physical properties and model employed must not only predict behavior accurately and distinguish between materials, but must also be readily comprehended by those who must use the model. We believe that the model proposed in this paper meets these requirements. It must be recognized that all the property data used to develop and apply the model are primary laboratory measurements independent of any EHD experiment.

One piece of apparatus (Figure 2) and some of the data (Figures

6, 8) were reported in last year's report (1) but are repeated here for clarity.

II. EXPERIMENTAL APPARATUS

Three different apparatus of basically two configurations were constructed and employed to measure the shear rheological response of lubricants to 1.2 GPa (180 kpsi). The two configurations will be referred to as the stress-strain apparatus, of which there are two, and the high shear stress viscometer. The high shear stress viscometer and one stress-strain apparatus operate to 0.7 GPa while the third device can operate at 1.2 GPa (180 kpsi).

The low stress pressure-viscosity data mentioned was measured in a traditional falling body viscometer which was developed under previous NASA support and reported before [1].

A. Stress-Strain Apparatus: 0.7 GPa

As reported previously [1], an apparatus was constructed to measure the mechanical shear properties of glassy lubricant samples to pressures of 0.7 GPa. It is shown schematically in Figure 2. The glassy sample is formed in an annular groove by cooling at elevated pressure. The groove is kept filled by a sample reservoir which is sealed from the working fluid (gasoline) by an isolator piston. The sample material can be sheared in the annulus by the development of a pressure difference across the driving piston. The shear stress is determined by knowing the geometry and measuring the differential pressure by two pressure transducers. The sample strain is determined by the displacement of the driving piston measured with an LVDT. This signal can also be used to measure the strain rate. The shear stress (pressure difference) and the strain (piston displacement) are recorded

on an x-y recorder. Sample temperature is determined by a thermocouple imbedded in the pressure vessel wall.

At moderate working temperatures, such as those for 5P4E (-20 to 35C), and elevated pressures, the seal friction is negligible and no shearing force across the piston can be maintained when the test material is above its glass transition temperature. However, with N1* the temperature required to go into the glassy region at moderate pressures is so low (-40C) that a correction for seal friction must be employed. The seal friction at low temperature was calibrated by using gasoline as the test fluid which has very low viscosity at the test temperature and pressure. Therefore, at the low shearing rate of the experiment, the driving force on the piston was assumed to be due to seal friction. This seal friction was typically less than five percent of the maximum shear stress measured for N1.

Referring to Figure 2 the sequence of a typical experiment is the following: with the sample in the apparatus, the system is heated to a temperature high enough to keep the sample in its liquid region at the predetermined pressure to be used. The system is then brought up to pressure with the valve open insuring uniform pressure throughout the apparatus. The system is then cooled to the desired temperature at or below the dilatometric liquid-solid transition while maintaining constant pressure. The isolating piston movement accommodates sample volume change during these state changes. The valve is then closed isolating the regions above and below the

*The fluids are described in the Appendix.

driving piston. Stress is applied to the sample by either increasing or decreasing the pressure on the bottom of the driving piston by varying the supply pressure. The pressure difference is measured by the two pressure transducers. The driving piston displacement and velocity are measured by the LVDT. By the nature of the device, when the piston moves downward the pressure level decreases and when it moves upward the pressure level increases. As will be shown, these pressure level changes are reflected in plastic shear stress response of the material. The pressure level changes can be kept to a minimum by keeping the strain (piston displacement) small for a given measurement.

B. Stress-Strain Apparatus: 1.2 GPa

The high pressure apparatus is shown schematically in Figure 3. The intensifier piston is driven into the high pressure chamber increasing the pressure of the working fluid and test sample. The device is assembled and filled so that the intensifier piston reaches the push piece when the desired pressure level is attained. The pressure on the low pressure side of the intensifier and the piston displacement are measured continuously on an x-y recorder. The plot of pressure-displacement follows a characteristic compression curve for the pressurizing medium until the push piece is contacted at which time the pressure deviates from the compression curve as a result of the shear force in the sample. This deviation permits determination of the shear stress in the sample and the piston displacement gives the strain.

C. High Shear Viscometer: 0.7 GPa

The high shear viscometer can operate to pressures of 0.7 GPa (100 kpsi) and is shown schematically in Figure 4. The sample is sheared between the central rod and the cylindrical hole. The rod is moved axially through the hole by a pressure difference imposed across a driving piston attached to the rod. The pressure difference is measured and is proportional to the shear stress. The rod displacement and velocity are measured by an LVDT permitting determination of the strain and strain rate. All signals are recorded on an x-y recorder. The pressure differential is small compared to the pressure level in the system. Volume changes of sample on each end of the shear area are compensated for by the isolating piston, diaphragm and a passage connecting the sample volume on either side of the shearing area.

III. LUBRICANTS INVESTIGATED

The seven materials investigated are listed in Table I. The naphthenic mineral oil (N1) and the polyphenyl ether (5P4E) are the same materials used in several publications from this laboratory on pressure-viscosity characteristics [cf. 8] and EHD film thickness and temperature measures [cf. 9, 10]. N1, 5P4E, and Santotrac 50 were studied previously [1,2] for solid-liquid transition under pressure. LVI260, VITREA 79 and TURBO 33 samples were received from K. L. Johnson who has published EHD on them [cf. 3,6,7]. Details of several properties of these materials are given in Appendix A.

Table I. Experimental Materials

Symbol	Description
N1	Naphthenic Base Mineral Oil
5P4E	Five ring polyphenyl ether
Santotrac 50	Synthetic Cycloaliphatic Hydrocarbon Traction Fluid
DMS	Dimethyl Silicone
LVI 260	Low Viscosity Index Mineral Oil
VITREA 79	High Viscosity Mineral Oil
TURBO 33	Plain Mineral Oil

IV. EXPERIMENTAL RESULTS

The experimental data obtained take several forms all originating from x-y recorder plots of stress and strain on the sample. Two representative plots are shown in Figures 5-7 which were obtained from the first apparatus described above. Similar records are obtained from the high shear viscometer. In both cases, to measure shear rates, an electrical signal of known frequency is superposed on the LVDT signal. The displacement per cycle of signal gives the strain rate. The superposed signal is not shown in Figures 5-7 for clarity and would simply appear as a small amplitude single frequency noise on the signals shown (similar to a 60 cycle AC pickup noise).

A. Shear Stress-Shear Strain Measurements

Figure 5 shows a typical hysteresis stress-strain diagram for 5P4E at 275 MPa (40 kpsi) and 18.4C. The low rate dilatometry transition temperature for 5P4E is 38C at 275 MPa [1]. Positive strain in Figure 5 corresponds to downward movement of the piston (Figure 2) which results in a system pressure decrease while negative strain occurs with upward movement of the piston resulting in an increase in system pressure. These system pressure changes cause the yield shear stress to decrease and increase respectively causing the different slopes in the two directions. Shearing starts at position 1 and proceeds sequentially through 10 with several reversals of stress application. Portions of the curve marked 2-3, 5-6 and 8-9 are artifacts of the system. They represent viscoelastic recovery of the material coupled with apparatus system response while the driving

force is being reversed.

Figure 5 shows that this material (5P4E) exhibits reversible elastic as well as plastic and viscous behaviors. The maximum shear stress it can with stand is about 50 MPa and the maximum elastic strain is small. The strain rates in this experiment were small (about $10^{-3}s^{-1}$) and varied somewhat from step to step. As will be shown below, the shear rate influences the shear stress until a maximum value is reached.

Figure 6 is also an x-y recorder plot for an experiment in which more control was exercised. The data was taken in a manner similar to that described above but with a single stepwise traverse of the piston as the apparatus temperature was brought stepwise up from -27C to 40C. When an equilibrium temperature was reached at each indicated temperature the stress was applied at a constant rate for the strain shown. The stress was then removed, the temperature changed and the recorder pen repositioned. The strain rate in these experiments was also about $5 \times 10^{-3}s^{-1}$ and was changing during the -27C measurement which accounts for the irregular appearance of that data. If the temperature is held constant, at say 20C, the curve shapes for increasing shear rate are like those for decreasing temperature. The elastic shear modulus, G_∞, and the yield shear stress both increase with increasing rate until maximum values of each are reached.

Several points of interest are apparent from Figure 6. At the low rate of the measurement no elastic or plastic behavior is

apparent above the liquid-solid transition temperature (38C [1]). The maximum elastic shear strain is only about 5 percent or less. And both the elastic shear modulus and plastic yield stress increase to a maximum at about 50C below the transition temperature.

Figure 7 shows that the yield stress remains nearly constant for much larger strains than shown in Figure 6. When the measurement shown in Figure 7 was made, care was taken to maintain a constant pressure level in the apparatus unlike the situation discussed above and shown in Figure 5. Therefore the decrease of stress with large strain shown in Figure 5 are truly artifacts of the apparatus.

A.1 Elastic Shear Modulus

The elastic shear modulus from the data presented in Figure 6 is shown in Figure 8. It is seen to approach asymptotically a limiting value of about 1.2 GPa. From Figure 6 it is seen that the elastic recoverable strain is about four percent. The value of elastic shear modulus has been the subject of much debate among people in the EHD field [11,7] with predictions from traction measurements typically one third to one tenth that measured in ultrasonic shear measurements [12,13]. The value reported in Harrison [13] from Barlow et al. [12] for 5P4E at 275 MPa is 1.2 GPa, essentially the same as that measured here. The ultrasonic measurements are for strains orders of magnitude smaller than those used here and for strain rates orders of magnitude higher, yet the limiting elastic shear modulus, G_∞, is the same.

The elastic shear modulus (G_∞) of 5P4E at several other temperatures and pressures and low shear rates ($10^{-2}s^{-1}$) are shown in Figure 9. In all cases they reach a maximum value as temperature

is decreased. Although it is not apparent from this figure, there is an increase of the shear modulus with pressure.

Data similar to that shown in Figure 6 have been taken at several additional pressures to 590 MPa (85 kpsi) on 5P4E, and on the naphthenic mineral oil (N1) and the synthetic cycloaliphatic hydrocarbon (Santotrac 50) to similar pressures. The yield shear stress was reported for these materials at several pressures and temperatures previously [1].

B. Shear Stress-Shear Strain Rate

It was found during the course of these experiments that, if the rate of the experiment was increased, the yield shear stress near the transition temperature increased and approached the value measured farther into the solid region. Therefore a series of experiments were performed with the device shown in Figure 2 in which the temperature was held constant (40C) and the shear rate varied for several pressures to 550 MPa. These data for 5P4E are plotted as shear shear stress - shear strain rate curves in Figure 10. (The left hand set of curves.) In each case the shear stress approaches a maximum value.

B.1 High Shear Stress Viscometry

The maximum value of shear stress attained in the solid region would also be reached in the liquid region (based on dilatometry) at very low shear rates relative to these normally encountered in an EHD contact. It is reasonable to expect that if the material has a limiting shear stress in the solid region, it will not withstand a higher stress in the liquid region. Therefore the viscometer shown in Figure 4 was used to measure the shear stress as a function of shear rate on the liquid side of the transition (See Figure 1).

These data for 5P4E at 40C are also shown in Figure 10 for three pressures (right hand group of data). Again the material exhibits a limiting shear stress. Over the entire range of pressures and two devices the limiting shear stress is seen to increase somewhat with presusre at constant temperature. A relatively straightforward analysis will show that these limiting shear stresses (which can be viewed as a reduction in viscosity) are not the result of viscous heating. The energy input rate of the process is too low.

A plot such as Figure 10 is sometimes referred to as a flow diagram. A straight line slope of plus one would represent a Newtonian viscous fluid. The data from the high shear viscometer shows this behavior as the shear rate is decreased and that of the stress-strain device approaches it at lower shear rates. The values of viscosity which these 45 degree lines represent agrees well with traditional falling body viscometer data where the pressures and temperatures overlap. They also permit the extension of the log-viscosity pressure isotherms to extremely high viscosities (of the order of 10^9 Pas).

The large strain visco-plastic behavior shown in Figure 10 can also be presented as an apparent viscosity as a function of shear rate in Figure 11. This figure contains two types of measurements; low shear rate falling body viscosity [1] and high stress viscosity measurements. The agreement between the measurements is apparent and the decrease in apparent viscosity along a line of constant shear stress is also clear. This is inherent material behavior and not viscous heating which would cause the inflexion of the apparent

viscosity curve to occur at the line of constant energy input rate per unit volume (shear stress times shear rate). Figure 11a is for 5P4E and 11b for Santotrac 50.

The above two types of viscosity measurement (Figure 11) and the yield shear stress data such as that in Figure 6 are shown in Figure 12a,b for 5P4E at 40C and 60C respectively and in Figure 13 for Santotrac 50 at 20C. In these figures for the large strain behavior, the data in the upper left hand group was obtained in a high stress low rate device, that in the upper right hand group was obtained in a high stress-high rate device, and that at the bottom was obtained in a standard falling body viscometer which is a very low constant stress device [1]. On this type of plot Newtonian viscous behavior is represented by a straight line with slope of one. Therefore it is seen how the viscometer and high stress data complement each other. The limiting shear stress increases somewhat with pressure but the effect is small on the scale of these figures.

C. Limiting Shear Stress

Figures 14a and b present the limiting shear stress for 5P4E as a function of temperature and pressure respectively. The dependence of the limiting shear stress in the ranges studied is nearly linear in each case and much less dependent than the low shear rate viscosity which tends to have an exponential dependence on both temperature and pressure.

Figures 15a and b show similar data for the synthetic cycloaliphatic hydrocarbon (Santotrac 50) behavior which in general is similar to 5P4E except the limiting shear stress tends to have

a greater dependence on pressure. Also shown in Figure 15b are two data points from the high pressure low shear rate device at about 1 GPa pressure. They are for Santotrac 50 at 11C and N1 at 17C.

Figure 16 presents limiting shear stress data for all three materials at 550 MPa (80 kpsi) as a function of temperature. These data indicate that in general the limiting shear stress decreases with temperature and the dependence varies with material. Depending on the temperature and pressure range of operation different materials will given the maximum traction transmitted in an EHD contact. Figure 16 should not be used to predict relative traction of these materials except at the pressure shown because the pressure dependence of the limiting shear stress differs considerably among the three fluids. At a somewhat higher pressure 5P4E and Santotrac 50 reverse relative positions.

Also shown in Figure 16 is a single data point for a dimethyl-siloxane (10^2 Pas at 27C) which shows a very low limiting shear stress (4 MPa) compared to the other three materials. In an EHD contact a shear stress this low would most likely be reached in the inlet zone. Therefore it would limit the ability of the contact to draw the material in and hence reduce the expected EHD film thickness. This may explain the long recognized difficulty of using this material as an EHD lubricant. This material and mechanism deserves further study.

Figure 17 presents the limiting shear stress at 0.55 GPa for the fluids received from K. L. Johnson (Vitrea 79, LVI 260). The data shown for 5P4E is that measured on our sample previously.

Although we received a 5P4E sample from K. L. Johnson, we only measured the kinematic viscosity of it. That measurement and discussions with K. L. Johnson regarding the history of their sample lead us to believe they are the same material. The limiting shear stress of Tribo 33 was not measured because the low viscosity of this material would require a shear rate beyond the capabilities of our equipment.

Figure 18 contains the low stress pressure viscosity data we measured in the falling body device on the samples received from K. L. Johnson (the same comments in the previous paragraph regarding the 5P4E apply also to these data).

V. DISCUSSION OF EXPERIMENTAL OBSERVATIONS

A. Relation to EHD Contacts

The results presented show the three materials exhibit viscous, elastic and plastic limiting shear stress behavior in a range of pressure and temperature which may occur in EHD contacts. The materials can exhibit any one or all three types of behavior in EHD contacts depending on the combinations of pressure, temperature and shear rate. Depending on these independent variables and how they are changed in an EHD experiment the material could undergo visco-elastic, visco-plastic, and/or elastic-plastic transitions in a given experiment without any recourse to thermal effects. This may account for the conflicting rheological models based on EHD experiments which are found in the literature.

The recoverable elastic strain is so small that elastic behavior is probably only important in EHD contacts for very small slide-roll ratios. The plastic or limiting shear stress begins at such small strains (the recoverable elastic limit) that it may be a dominant feature of the rheological response of most materials in EHD contacts.

As we reported previously [1,2] the temperature at which liquid-solid transition occurs for low rate processes increases with pressure sufficient to insure solidlike behavior in many EHD contacts with many common materials. The transition was referred to as the glass-transition [1,2] which is correct but misleading in that these materials have a low yield shear stress and are very ductile under pressure compared to that behavior which is normally

associated with common glasses. Therefore we will now refer to it as the solid-liquid transition. The rate of environmental change in an EHD contact is greater than that in the dilatometry experiment. This rate increase will shift the liquid-solid transition to increase the pressure-temperature region associated with the solidlike behavior. Therefore the dilatometry based transition measurements can be viewed as a bound on the lubricant behavior.

Johnson and Roberts[6] report liquid-solid transitions in an EHD contact based on traction measurements under well controlled and novel kinematics. They observed transitions by varying pressure at constant temperature and by varying temperature at constant pressure. The lubricant employed was not identical to any of those reported in [1,2] but in [1,2] we showed that several mineral oil based materials had very similar transition characteristics. The Johnson and Roberts [6] material was similar to but a higher viscosity than our naphthenic mineral oil (N1). The dilatometry transition data for our mineral oils is shown in Figure 1 along with the EHD based transition points of Johnson and Roberts [6] and Johnson and Cameron [3]. The agreement between the two different kinds of measurements lends credibility to the relevance of the dilatometry data to EHD applications.

Figure 19 is a heuristic diagram indicating how this solid-liquid transition might influence EHD contacts for three representative lubricants [1,2]. If the transition occurs in the Hertzian zone, it would be expected to influence the contact traction while, if it occurs in the inlet zone, it would also affect the film

thickness. As seen in Figure 19, 5P4E is the most likely to experience the transition not only in the Hertzian zone but also the inlet zone at least at moderate temperatures. The transition of the mineral oil will only occur in the inlet zone for low temperature applications and in the Hertzian zone for higher pressure applications. The synthetic paraffin mineral oil (XRM 177) is far less likely to experience the transition in the inlet zone and it will occur in the Hertzian zone only for very high pressure contacts.

B. Relation to Lubricant Shear Behavior

The above leads one to ask about the shear rheological properties in the solid region and near the transition zone for the magnitude of strain expected in an EHD contact. In the liquid region the shear rheological behavior would be expected to be classical viscous behavior with possible viscoelastic phenomena at high rates of change of stress. Well into the solid region elastic behavior for small strains would be expected with some limit to the elastic stress and strain that the material can withstand before yielding. Near the transition curve the behavior would be expected to be some complex combination of viscous, elastic, and plastic behavior. In determining the shear rheological behavior of lubricants we must determine what is meant by "well into", "near", "small strain", and "high rates of change of shear stress", relative to the lubricants employed and concentrated contact kinematics and dynamics.

The shear rheological measurements shown above cover the solid region, near the transition curve and the viscous region at low shear stress. The materials exhibited classical elastic behavior for small

strains, limiting yield shear stress for large strains and large stresses, and viscous behavior for large strain small stress. The latter case agrees well with ordinary falling body viscosity data. The viscous, elastic, and plastic characteristics of the materials can be unified into a straightforward Maxwell model with non-linear viscosity. The primary rheological properties will then be employed in the model to predict EHD traction.

The elastic-plastic behavior of 5P4E shown in Figures 5-7 is typical of shear stress-shear strain behavior in the solidlike region of behavior. The limiting elastic shear modulus, $G_\infty(T,p)$ (Figure 8) measured on 5P4E at 275 MPa is 1.2 GPa and agrees with that measured ultrasonically by Barlow [14] at the same pressure and a much higher rate. The recoverable elastic strain is only about 0.03 which is small compared to that occurring in most EHD contacts at moderate to high slide-roll ratios. For larger strains the material exhibits a yield shear stress which reached a maximum value as the shear rate was increased. The limiting shear stress, τ_L, and the limiting shear modulus, G_∞, are related through the maximum recoverable elastic shear strain, γ_{RE}, by the approximate relation

$$\tau_L = G_\infty \gamma_{RE} \quad . \tag{1}$$

Therefore the limiting yield shear stress is about a factor of thirty less than the elastic shear modulus.

VI. UNIFICATION OF THE SHEAR RHEOLOGICAL MEASUREMENTS

The pattern of the data in Figures 11 through 13 suggests a straight-forward shifting of the data by non-dimensionalization. The shear stress can be non-dimensionalized by dividing by the maximum or limiting yield shear stress, $\tau_L(p,T)$, and the shear rate can be non-dimensionalized by multiplying by the low shear stress viscosity, $\mu_o(p,T)$ and dividing by the limiting yield shear stress, $\tau_L(p,T)$. The non-dimensionalized data from both Figures 12 and 13 are presented in Figure 20.

A. Physical Interpretation

Several physical interpretations can be given to these dimensionless parameters. The dimensionless shear stress, $\hat{\tau} = \frac{\tau(p,T)}{\tau_L(p,T)}$ (ordinate) is the ratio of the actual shear stress to the limiting yield shear stress the material can withstand at the given temperature and pressure. The dimensionless shear rate, $\hat{\dot{\gamma}} = \frac{\dot{\gamma}\mu_o(p,T)}{\tau_L(p,T)}$ (abscissa), can be thought of as: a) the ratio of the shear stress that would prevail if Newtonian viscous behavior was followed, to the limiting yield shear stress; b) as the actual shear rate times a visco-plastic flow relaxation time t_p, where $t_p \equiv \frac{\mu_o(p,T)}{\tau_L(p,T)}$, or c) the dimensionless shear rate might also be thought of as a Deborah number of visco-plastic transition because $\hat{\dot{\gamma}} = 1$ is the middle of the transition from Newtonian viscous behavior ($\hat{\dot{\gamma}} << 1$) to limiting shear stress plastic flow behavior ($\hat{\dot{\gamma}} >> 1$). Yet another interpretation

might be that the dimensionless shear rate is the time derivative of the shear strain scaled to the recoverable elastic strain with respect to a dimensionless time obtained by scaling time with the elastic relaxation time.

The visco-plastic flow relaxation time is related to the visco-elastic relaxation, $t_e = \frac{\mu_o(p,T)}{G_\infty(p,T)}$ by the recoverable elastic shear strain γ_{RE}

$$t_p = \frac{\mu_o(p,T)}{\tau_L(p,T)} \cdot \frac{G_\infty(p,T)}{G_\infty(p,T)} = t_e \frac{G_\infty(p,T)}{\tau_L(p,T)} = t_e \frac{1}{\gamma_{RE}} \qquad (2)$$

or

$$\gamma_{RE} = \frac{t_e}{t_p} \quad .$$

As we have shown above, the recoverable elastic shear strain is about 0.03. Therefore the visco-plastic relaxation time is about 30 times longer than the visco-ealstic relaxation time.

B. Proposed Flow Model

The flow data shown in Figures 11 through 13 and non-dimensionalized as described above are shown in Figure 20. It shows that this approach coordinates the measured data over a wide range of pressures and temperatures as well as over many orders of magnitude of shear stress and shear strain rate for both materials. The visco-plastic data can be described reasonably well with a single natural log function. The relationship proposed for the large strain flow behavior is

$$\hat{\dot{\gamma}} = - \ell n(1 - \hat{\tau}) \tag{3}$$

and is shown as the solid curve in Figure 20. This can be reviewed as a non-linear viscous flow equation.

If this relation is introduced as the viscous part of the usual Maxwell visco-elastic model, we get a modified Maxwell model of

$$\hat{\dot{\gamma}} = \hat{\dot{\gamma}}_e + \hat{\dot{\gamma}}_v \tag{4}$$

or

$$\hat{\dot{\gamma}} = \hat{\dot{\tau}} - \ell n(1 - \hat{\tau}) \tag{5}$$

where $\hat{\dot{\gamma}}$ and $\hat{\tau}$ are described as above and

$$\hat{\dot{\tau}} = \frac{\mu_o}{\tau_L G_\infty} \frac{d\tau}{dt} = t_e \frac{d\frac{\tau}{\tau_L}}{dt} = \frac{d\frac{\tau}{\tau_L}}{d\frac{t}{t_e}} = \frac{d\hat{\tau}}{d\hat{t}} \tag{6}$$

Equation (5) is the dimensionless form of the proposed shear rheological equation and is shown in Figure 21. Where all three kinds of behavior are seen.

The dimensionless form of the proposed modified Maxwell Model, Equation 5, obscures the familiar primary physical data required to implement it. Equation (7) is a dimensional form of the model

$$\dot{\gamma} = \frac{1}{G_\infty} \frac{d\tau}{dt} - \frac{\tau_L}{\mu_o} \ell n \left(1 - \frac{\tau}{\tau_L}\right) \tag{7}$$

From Equation 7 it is seen that the three primary physical properties required to use the model are low shear stress viscosity μ_o, the limiting elastic shear modulus, G_∞, and the limiting yield shear stress, τ_L, all as functions of temperature and pressure. By the relationships mentioned previously either or both of the last two (G_∞ and τ_L) could be replaced by one or two of the following three properties; visco-elastic relaxation time (t_e), visco-plastic relaxation time (t_p), or recoverable elastic strain (γ_{RE}). The three primary properties (μ_o, G_∞, τ_L) are probably the most logical to pursue.

Several techniques have been available for some time to measure μ_o and G_∞ and the measurement of τ_L is relatively straightforward as described above. We have the capability of measuring all three of these properteis over a range of pressures and temperatures.

VII. APPLICATION OF THE MODEL TO EHD TRACTION PREDICTIONS

We have employed the above model to predict shear stress and traction in EHD point contacts. The properties used are the three primary material properties mentioned above and measured in our laboratory. The contact was divided nonuniformly into a grid of 20 segments on a cord in the direction of motion and 20 such strips across the contact perpendicular to the direction of motion to permit pressure and material property variation in the contact. The following assumptions were employed; the film thickness and material temperatures were assumed uniform throughout the contact, the pressure distribution was Hertzian, no twist or side slip was present, the viscosity was an exponential function of pressure, the elastic shear modulus was constant, and the elastic surface compliance was proportional to the contact traction as developed by Kalker [15] and reported in Johnson and Roberts [6], and inlet zone effects were neglected. Several of these assumptions can be called into question and should be refined in subsequent development particularly those concerned with the temperature distribution and the inlet zone influence. However, they are acceptable for a first test of the model and seem to be justified as the results will show.

Although we know the film temperature is not constant, the analysis is done for slide-roll ratios of less than one tenth. From other work in this laboratory [1,16,17] under conditions similar to those used in this analysis we know the maximum surface temperature rise is usually less than 5C above the bulk temperature in this

range of operating conditions. Although we have not measured lubricant temperatures at these low slide-roll ratios, work in sliding contacts would indicate they are probably less than 5 to 10C above the surface temperature.

With the above assumptions a program was written to calculate the local shear stress at each point in the grid by using a Bisection Method on the model equation with starting shear stresses of zero and 0.999 τ_L. If the Bisection Method does not find a solution as the trial shear stress reaches 0.999 τ, the solution is assumed to be τ_L. To obtain the time derivative term, upstream grid positions plus a convective derivative are employed for a given grid point. The average shear stress in the contact is obtained by integration over the area and the traction coefficient is the ratio of the average shear stress divided by the average pressure.

A. Predicted Shear Stress Distributions

Figure 22 is a plot of the shear stress along the centerline in the direction of motion (from left to right) at various slide-roll ratios for Santotrac 50 at 20C, a Hertz pressure of 0.5 GPa, and a rolling velocity of 0.22 m/s. The film thickness used was 0.2 μm. As seen at the lowest slide-roll ratio the limiting shear stress is not reached, but at a slide-roll ratio of about 10^{-4} the limiting stress value is reached somewhat passed the center of the contact. As the slide-roll ratio is further increased the region where the limiting shear stress occurs grows as an area spreading outward to cover the entire contact. As seen from the traction coefficient

data, Figure 26, this growth of the limiting shear stress region is occurring while the traction is increasing linearly with slide-roll ratio to the maximum traction value. The variation of properties over the contact is important. In the cases shown in Figure 22 the shear stress is predominately viscous except where the limiting value is reached. This is primarily because of the pressure selected for the example (p_H = 0.5 GPa). At a higher pressure or lower temperature this material would also show elasto-plastic behavior as the 5P4E does in Figure 23.

Figure 23 shows the shear stress distribution for a similar calculation with 5P4E. In this case no viscous behavior is seen, only elastic and limiting shear stress plastic behavior. The area of limiting shear stress starts at the exit region and grows forward as the slide-roll ratio increases from about 10^{-4} to about 10^{-2} when the limiting shear stress occurs over the entire contact. The resulting traction coefficient as a function of slide-roll ratio for this case is also shown in Figure 26.

B. Limiting Case Traction Predictions

In the above cases we saw examples of visco-plastic and elasto-plastic behavior on shear stress distribution. It is instructive to take one of these materials and look at the predicted traction curve for various limiting cases of the model compared to the complete model. The viscoelastic case occurs by requiring the limiting shear stress to be very large compared to any shear stress value expected in the contact. Equation (7) of the model then becomes the classical Maxwell model of

$$\dot{\gamma} = \frac{1}{G_\infty}\frac{d\tau}{dt} + \frac{\tau}{\mu_o} \quad . \tag{7a}$$

The limiting case of visco-plastic results from specifying a very large value for G_∞ so the model becomes the non-linear viscous from

$$\dot{\gamma} = -\frac{\tau_L}{\mu_o} \ell n \left(1 - \frac{\tau}{\tau_L}\right) \tag{7b}$$

The third possibility of elastic-plastic behavior is obtained by letting the viscosity take on a very large value in which case all the strain at low stress occurs in the elastic term and at large stress the limiting stress controls. This special case model equation looks just like Equation 7. Any change in appearance would lose an essential feature. The traction slide-roll ratio curve predicted by these three special cases and the complete model are shown in Figure 24 for 5P4E at the conditions indicated. For this material and the conditions used, the essential features are the elastic behavior at low slide-roll ratio and plastic behavior at higher slide-roll ratio. The transition slide-roll ratio is only 10^{-3}, however, which is a small value and attained only in the better, well controlled traction devices. Neither the visco-elastic nor visco-plastic models are appropriate over the entire range. The influence of surface compliance is to shift the slide-roll ratio to increasing values. Surface compliance is included in all the calculations presented in this paper except the one curve so indicated in Figure 24. If it were not included

the curve so marked in Figure 13 would be predicted during the rise in traction coefficient for the full model. Once the peak traction is reached surface compliance effects can no longer be seen.

C. Comparison with Measured EHD Traction

The necessary test for a proposed model is the comparison of predicted values with measured values in an EHD traction device. As seen from the above predictions the most important parts of the curve to check are the low slide-roll ratio range and the maximum values. Our own traction device at this time does not have adequate control in crucial low slide-roll ratio range and therefore we must rely on the data in the literature of which there is a great deal (i.e., Cheng and Trachman [18], Dyson [11], Smith et al. [19], Hirst et al. [20] and Johnson et al. [6,3,7]). Any choice is complicated by the need to know the magnitude and precision of both operating conditions and the data as well as the relationship between the lubricant used and the material we used to determine the primary physical properties for the model. We therefore choose for the first comparison the data of Johnson and Tevaarwerk [7] on 5P4E. The material is well defined and the major possible variations would be lot-to-lot variation and contamination of either sample both of which we think were small.

Figure 25 is a plot of traction coefficient against slide-roll ratio for 5P4E at 1 GPa Hertz pressure and rolling velocity of 0.22 m/s. The data points are those reported by Johnson and Tevaarwerk [7] for a bulk temperature of 40C. The two solid curves are predicted

by the model using the film thickness to Hertz diameter in [7] and average film temperatures of 40C and 50C. (The curved marked 40C is from the same conditions used to develop the stress distributions shown in Figure 23. Both curves agree reasonably well with the data when the basis of the model and the difficulties encountered in attempting such a prediction in the past are considered. The 50C curve not only agrees with the data better than the 40C curve but also is a more reasonable assumption for the film temperature if the bulk temperature is 35C. We have shown elsewhere [16,17] that for these low slide-roll ratios, pressures and velocities the surface temperature will increase 5 to 8C above the bulk and the film must be somewhat higher. The agreement shown in Figure 25 indicates that the proposed approach to EHD traction is promising and deserving of further development.

Figure 26 shows the predicted traction curves for three materials for which we currently have a sufficient amount of primary data. Although the pressures and kinematics are the same for the three materials, the temperatures are different because of the ranges of material properties available. In the cases of N1 and Santotrac 50 a noticeable portion of the traction is the result of viscous action even at the higher slide-roll ratio. This accounts for the continued increase in traction for slide-roll ratio greater than 10^{-3}. The plastic flow zone is still spreading with increasing slide-roll ratio as shown in Figure 22. However, the 5P4E for slide-roll ratios greater than 10^{-3} has the entire area covered by the plastic flow

zone (Figure 23) and therefore only thermal effects or changing pressures will change the traction in that range. Hence the zero slope to the traction curve. Caution must be exercised in generalizing about the relative maximum traction shown for these three materials because the limiting shear stress dependence on temperature and pressure for the three materials is different.

As mentioned above, samples of fluid were received from K. L. Johnson and some properties were measured. The traction predicted from our model with those data for conditions reported by Johnson and Tevaarwerk [7] are shown in Figure 27b and can be compared with the measured tractions reported by Johnson and Tevaarwerk which are shown in Figure 27a. Although the predictions do not precisely agree with the measured values, the comparison is very promising. The model does properly rank the materials, predicts essentially the measured maximum traction, and the roll of slide-roll ratio where the maximum traction is reached.

D. Predicted Effective Viscosity in EHD Contacts

If we consider a material and set of conditions which produce primarily visco-plastic flow (such as shown in Figure 22), and consider an EHD experiment with increasing load and fixed kinematics, we could observe an effective viscosity of the material. This is essentially one of the experiments of Johnson and Cameron [3]. In our model (Equation 5) this would be comparable to considering constant shear rate, no elastic effects, and increasing pressure. The ratio of shear stress to shear rate is the apparent viscosity. The results of this calculation are shown along with the low stress pressure viscosity

for several constant shear rates in Figure 28. The lower the shear rate the higher the viscosity where the apparent viscosity begins to diverge from the low stress viscosity curve. The slope of the curve after the divergence is the limiting shear stress dependence on pressure. Data from Figure 12b are plotted on the curve for a shear rate of 100 s^{-1} and are seen to exhibit this behavior.

Figure 28 shows how the viscosity obtained from the high stress data (upper left hand part of Figure 12b) and that from the high stress viscometer (upper right hand part of Figure 12b) are consistent with the low shear stress falling body viscosity-pressure data for 5P4E at 60C. Also shown in Figure 28 are the apparent viscosities predicted at constant shear rate by the model. If the viscosity was measured as a function of pressure at the constant temperature and the steady shear rate given, it would follow the usual curve up to the point shown and then go off nearly horizontal. The lower the shear rate, the higher the point of departure. The slope of the curve after it departs from the low shear rate curve is the rate of change of the limiting shear stress with pressure.

VIII. CONCLUSION

We believe we have found and, at least partially, substantiated a simple visco-elastic-plastic material shear rheological model employing measured primary laboratory data which predicts measured EHD traction under typical operating conditions. The model incorporates the three classical forms of material shear behavior, Newtonian viscous, Hookean elastic and plastic yield. The identification of the controlling material properties (μ_0, G_∞, τ_L) will aid designers and material synthesizers because of the small quantities of material required to determine the properties. The limiting yield shear stress determines the maximum traction which can be transmitted in an EHD contact. The variation of that property with temperature and pressure will be important to contact traction behavior.

The results show how the transition to plastic yield influence the traction as the yielded region in the contact spreads. It was seen that the transitions toward the inlet region and therefore one would expect that as the transition moves into the inlet zone it may also influence the film thickness. The effect would most likely be to decrease the film thickness compared to the values predicted for the usual viscous material model. This has been studied by Wilson and Aggrawal [21] for metalworking and needs to be explored for elasto-hydrodynamic lubrication.

IX. REFERENCES

1. Winer, W. O., and Sanborn, D. M., "Surface Temperatures and Glassy State Investigations in Tribology", NASA CR 3031, (June 1978).

2. Alsaad, M., Bair, S., Sanborn, D. M. and Winer, W. O., "Glass Transitions in Lubricants: Its Relation to EHD Lubrication", ASME Paper No. 77-Lub-3 (to be published in Trans. ASME, Journal of Lubrication Technology (1978).

3. Johnson, K. L., and Cameron, R., "Shear Behaviour of Elasto-hydrodynamics Oil Films at High Rolling Contact Pressures", Proc. Inst. Mech. Engrs., 182, Pt. 1, pp. 307-319 (1967-68).

4. Smith, F. W., "Lubricant Behaviour in Concentrated Contact Systems - The Castor Oil-Steel System", Wear 2, No. 4, pp. 260-263 (1959).

5. Plint, M. A., "Traction in Elatohydrodynamic Contacts", Proc. Inst. Mech. Engrs., 182, Pt. 1, p. 300-306 (1967-68).

6. Johnson, K. L. and Roberts, A. D., "Observations of Visco-elastic Behavior of an Elastohydrodynamic Lubricant Film", Proceedings of the Royal Society of London, 337A, pp. 217-242 (1974).

7. Johnson, K. L., and Tevaarwerk, J. L., "Shear Behaviour of Elastohydrodynamic Oil Films", Proc. Roy. Soc of London, 356A, pp. 215-236 (1977).

8. Novak, J., and Winer, W. O., "Some Measurements of High Pressure Lubricant Rheology", Trans. ASME, Journal of Lubrication Technology, 90, No. 3, pp. 580-591 (1968).

9. Nagaraj, H. S., Sanborn, D. M., and Winer, W. O., "Surface Temperature Measurements in Rolling and Sliding EHD Contacts", ASLE Paper No. 78-AM-2B-2 (to be published in ASLE Trans. 1978).

10. Nagaraj, H. S., Sanborn, D. M., and Winer, W. O., "Direct Surface Temperature Measurements by Infrared Radiation in EHD, and the Correlation of the Blok Flash Temperature Theory", (to be published in Wear early 1978).

11. Dyson, A., "Frictional Traction and Lubricant Rheology in Elastohydrodynamic Lubrication", Philosophical Trans. Roy. Soc. of London, 266A, p. 1 (1970).

12. c.f. Barlow, A. J., Harrison, G., Irving, J. B., Kim, M. G., Lamb, J., and Pursley, N. C., "The Effect of Pressure on the Viscoelastic Properties of Liquids", Proc. Roy. Soc. of London, 327A, pp. 403-412 (1972).

13. Harrison, G., The Dynamic Properties of Supercooled Liquids, Academic Press (1976).

14. Barlow, A. J., Erginsav, A., and Lamb, J., "Vicsoelastic Relaxation in Liquid Mixtures", Proc. Roy. Soc. of London, 309A, pp. 473-496, (1969).

15. Kalker, J. J., Proc. K. Ned. Akad. Wet., B67, p. 135.

16. Nagaraj, H. S., Sanborn, D. M. and Winer, W. O., "Surface Temperature Measurements in Rolling and Sliding EHD Contacts", ASLE Paper No. 78-AM-2B-2 (to be published in ASLE Trans. 1978).

17. Nagaraj, H. S., Sanborn, D. M. and Winer, W. O., "Direct Surface Temperature Measurements by Infrared Radiation in EHD, and the Correlation of the Blok Flash Temperature Theory", (to be published in Wear early 1978).

18. Trachman, E. G., and Cheng, H. S., "Traction in Elastohydrodynamic Line Contacts for Two Synthesized Hydrocarbon Fluids", ASLE Paper No. 73LC-4A-1, (1973).

19. Smith, R. L., Walowit, J. A., and McGrew, J. M., "Elastohydrodynamic Traction Characteristics of 5P4E Polyphenyl Ether", Trans. ASME, Journal of Lubrication Technology, 95, pp. 353-362, (1973).

20. Adams, D. R., and Hirst, W., "Frictional Traction in Elastohydrodynamic Lubrication", Proc. Roy. Soc. of London, 332A, pp. 505-525, (1973).

21. Wilson, W. R. D., and Aggrawal, B. B., "A Plastohydrodynamic Inlet Zone Analysis for a Visco-Plastic Lubricant", Wear, 47, pp. 119-132 (1978).

APPENDIX

DESCRIPTION OF EXPERIMENTAL FLUIDS

Symbol:	N1	
Source:	Sun Oil Company	
Type:	Naphthenic Base Oil R-620-15	
Properties:	Viscosity at 37.8C, m^2/s	24.1×10^{-6}
	Viscosity at 98.9C, m^2/s	3.73×10^{-6}
	Viscosity Index (ASTM D-2270)	-13
	Flash Point, C	157
	Pour Point, C	-43
	Density at 20C, Kg/m^3	915.7
	Average Molecular Weight	305

Symbol:	5P4E	
Type:	Five-ring Polyphenyl Ether	
Source:	Monsanto Company	
Properties:	Viscosity at 37.8C, m^2/s	363×10^{-6}
	Viscosity at 98.9C, m^2/s	13.1×10^{-6}
	Density at 22.2C, Kg/m^3	1205
	Density at 37.8C, Kg/m^3	1190
	Flash Point, C	288
	Pour Point, C	4.4

Symbol:	Santotrac 50	
Source:	Monsanto Company	
Type:	Synthetic Cycloaliphatic Hydrocarbon Traction Fluid	
Properties:	Viscosity at 37.8C, m^2/s	34×10^{-6}
	Viscosity at 98.9C, m^2/s	5.6×10^{-6}
	Pour Point, C	-37
	Density at 37.8C, Kg/m^3	889
	Flash Point, C	163
	Fire Point, C	174
	Specific Heat at 37.8C, J/Kg·K	2332
	Additive package includes: Antiwear (zinc dialkyl dithiophosphate), Oxidation inhibitor, Antifoam, VI Improver (Polymethacrylate).	

Symbol:	Turbo 33	
Source:	Shell Oil Company (via K. L. Johnson)	
Type:	HVI low viscosity oil	
Properties:	(From K. L. Johnson)	
	Viscosity at 37.8C, m^2/sec	60.3×10^{-6}
	Viscosity at 98.9C, m^2/sec	7.8×10^{-6}
	Density at 15.5C, kg/m^3	889
	Specific gravity 60/60F	0.889
	Viscosity pressure coefficient at 37.8c, m^2/N	20.6×10^{-9}

Symbol:	Shell Vitrea 79	
Source:	Shell Oil Company (Via K. L. Johnson)	
Type:	HVI high viscosity oil	
	Predominantly naphthenic and paraffinic	
Properties:	(From K. L. Johnson)	
	Viscosity at 37.8C, m^2/sec	581×10^{-6}
	Viscosity at 98.9C, m^2/sec	75×10^{-6}
	Density at 15.5C, kg/m^3	886
	Specific gravity 60/60F	0.886
	Viscosity pressure coefficient at 37.8C, m^2/N	25×10^{-9}

Symbol:	LVI 260	
Source:	Shell Oil Company (via K. L. Johnson)	
Type:	LVI High Viscosity Oil	
	47% saturates and 53% aromatics	
Properties:	(From K. L. Johnson)	
	Viscosity at 37.8C, m^2/sec	338×10^{-6}
	Viscosity at 98.9C, m^2/sec	232×10^{-6}
	Density at 15.5C, kg/m^3	929
	Specific gravity 60/60F	0.929
	Viscosity pressure coefficient at 37.8C, m^2/N	34.2×10^{-9}

Symbol:	DMS	
Source:	Dow Corning Corporation	
Type:	*Dimethyl Siloxane* DC-200-10^{5}	
Properties:	Viscosity at 25C, m^2/sec	1×10^{-1}

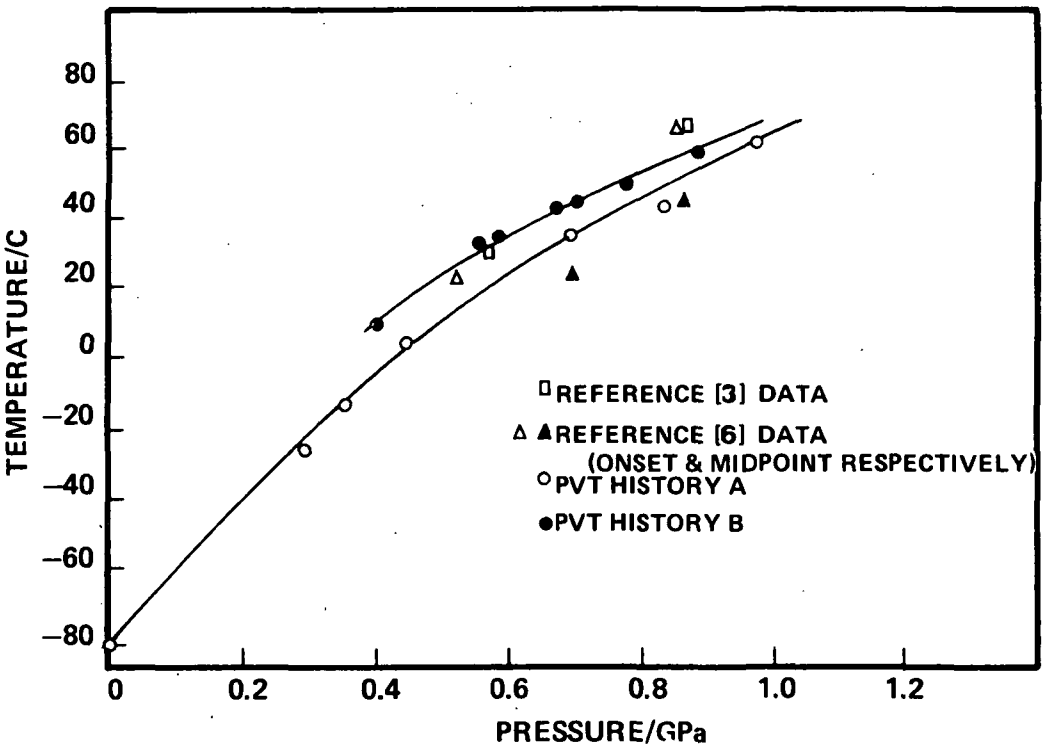

Figure 1. Comparison of glass transition of N1 by various methods

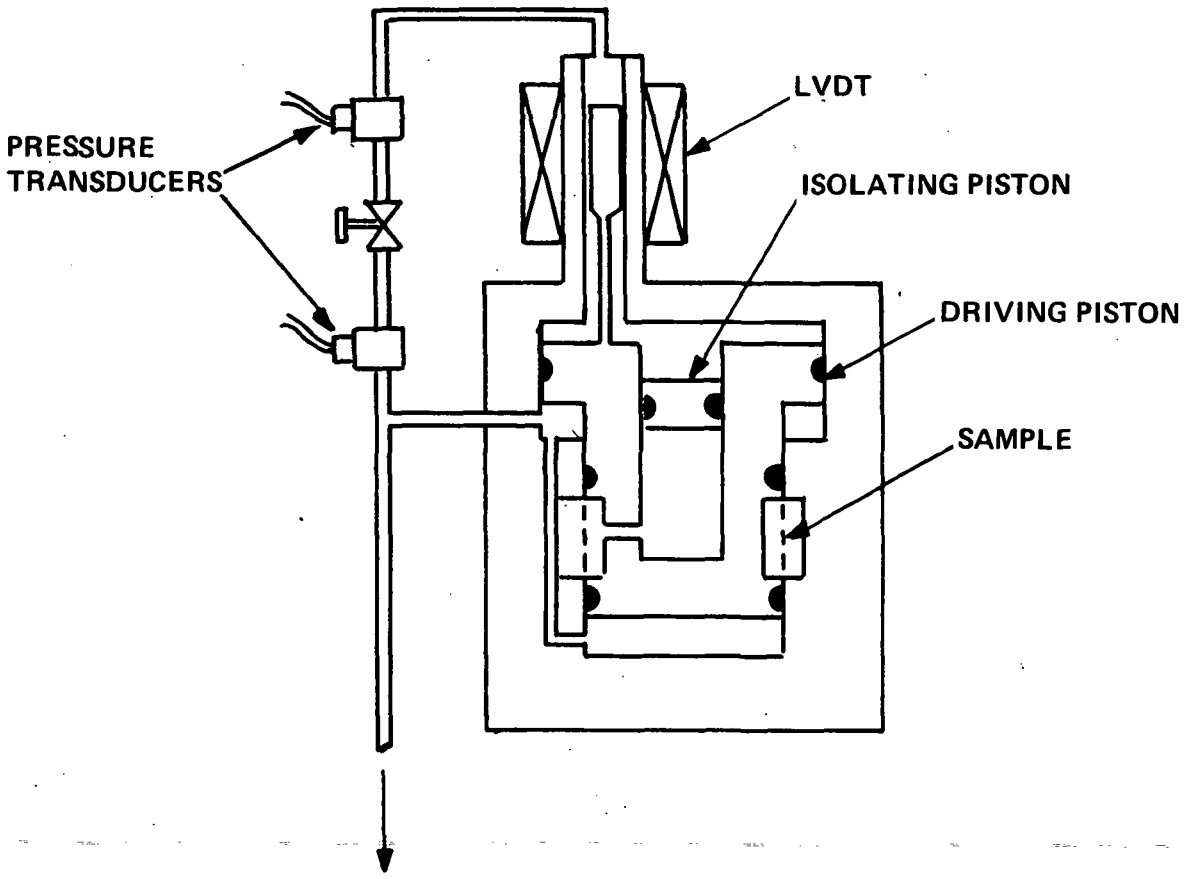

Figure 2. Schematic of shear stress apparatus, 0.7 GPa (100 kpsi).

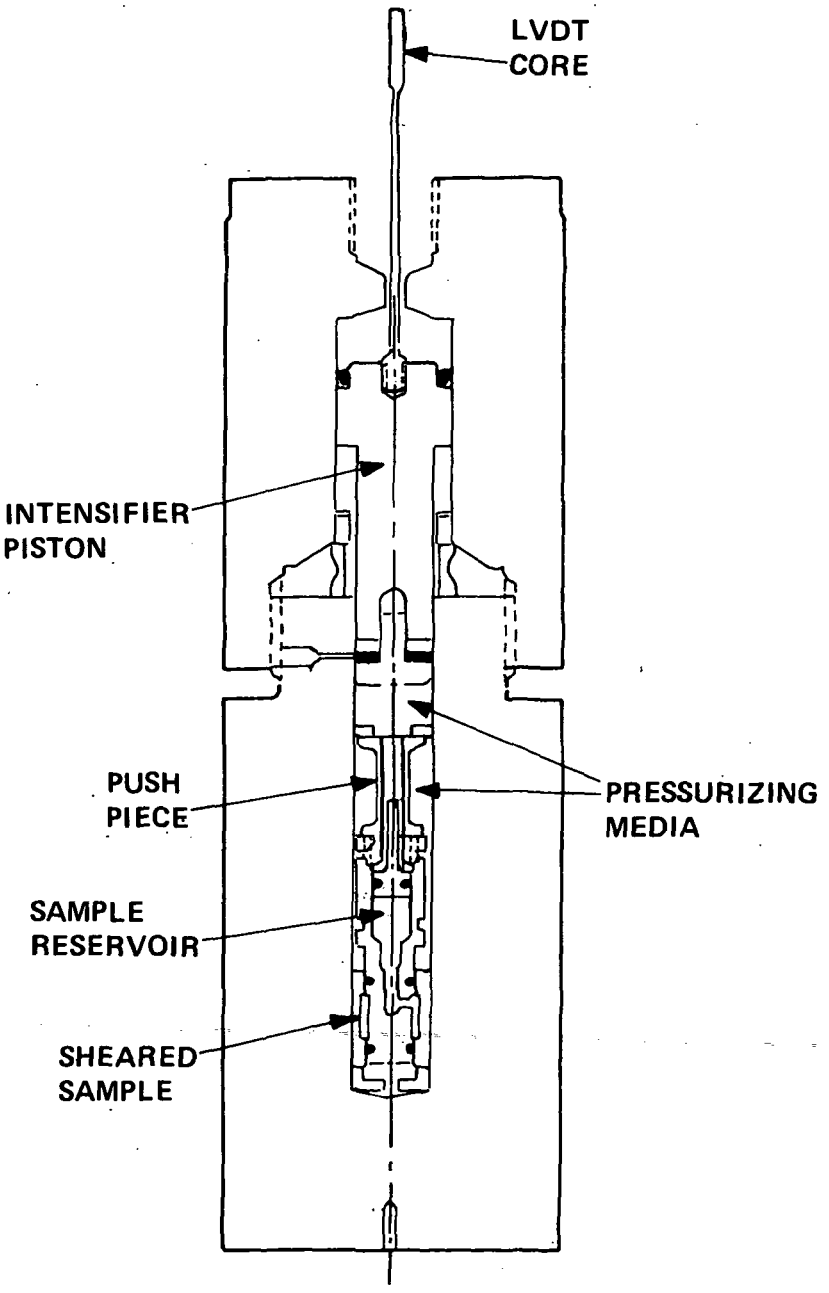

Figure 3. Schematic of high pressure shear stress apparatus (1.2 GPa)

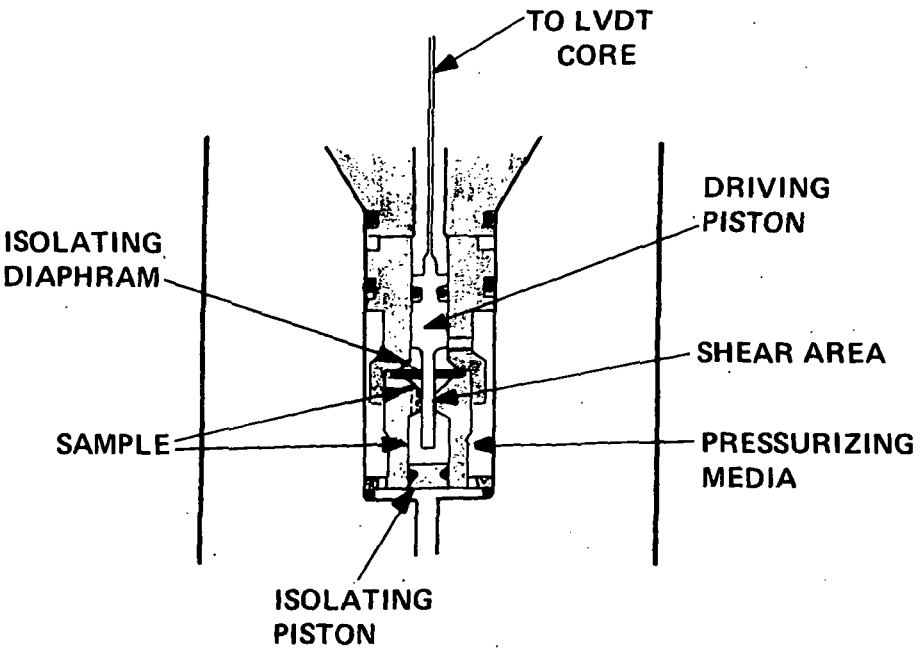

Figure 4. Schematic of high shear stress viscometer (0.7 GPa)

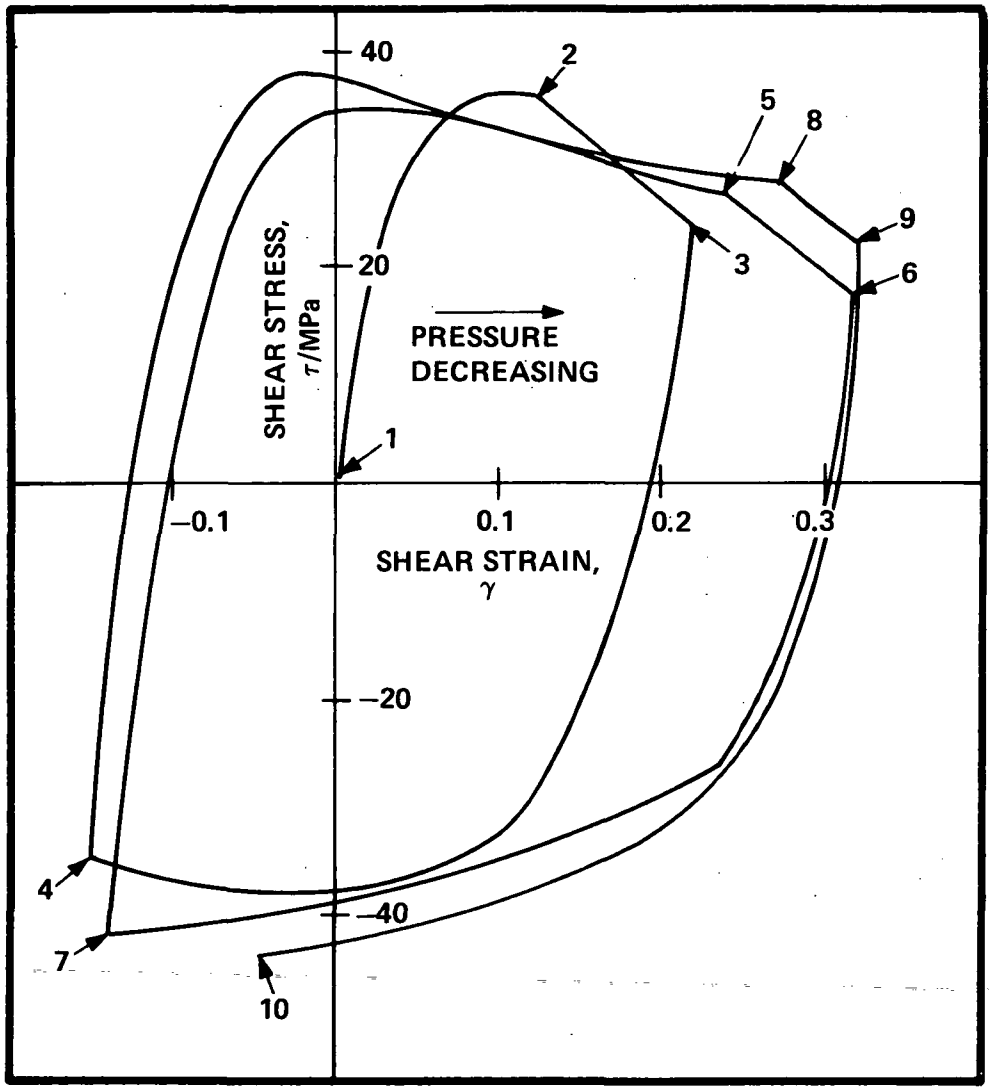

Figure 5. Shear stress strain hysteresis loops, 5P4E, 275 MPa, 18C. Strain rate variable

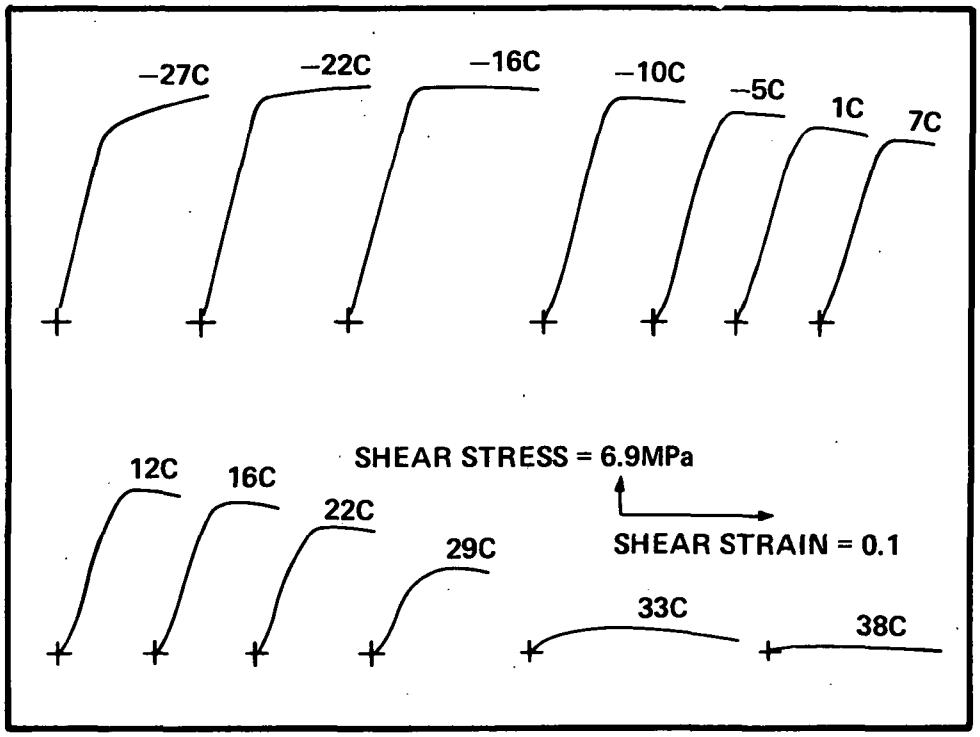

Figure 6. Recorder plot of shear stress versus shear strain for polyphenyl ether (5P4E) at 0.275 GPa (40 kpsi) and indicated temperatures

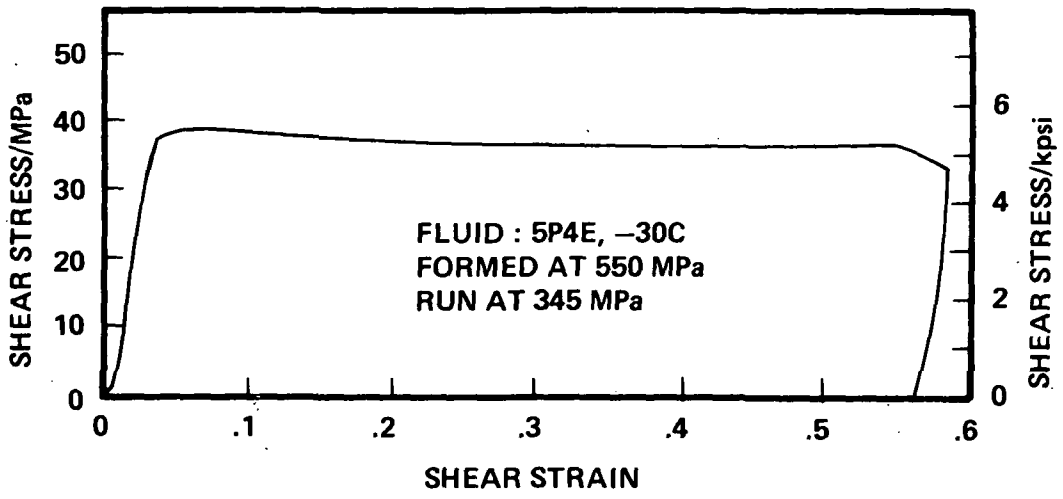

Figure 7. Shear stress-shear strain for 5P4E at -30C and 345 MPa (50 kpsi) after amorphous solid formation at -30C and 559 MPa (80 kpsi)

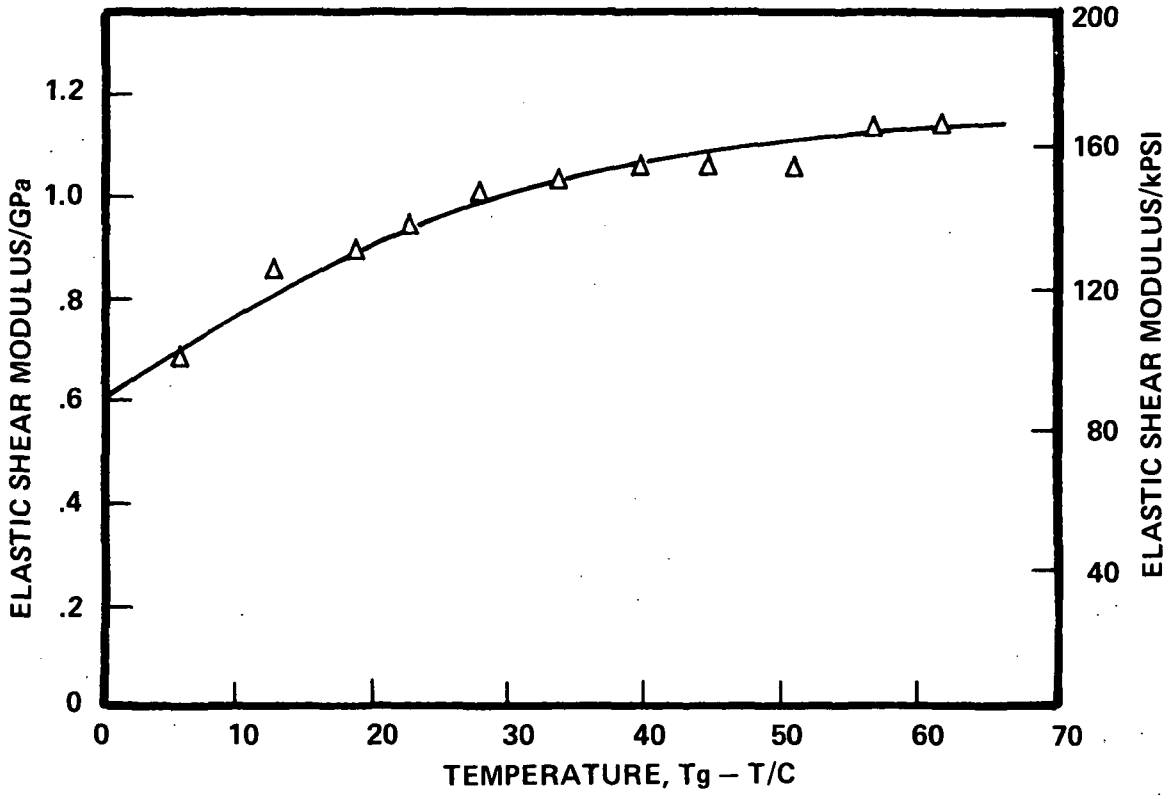

Figure 8. Elastic shear modulus of polyphenyl ether (5P4E) at 0.275 GPa (40 kpsi) in amorphous glassy region

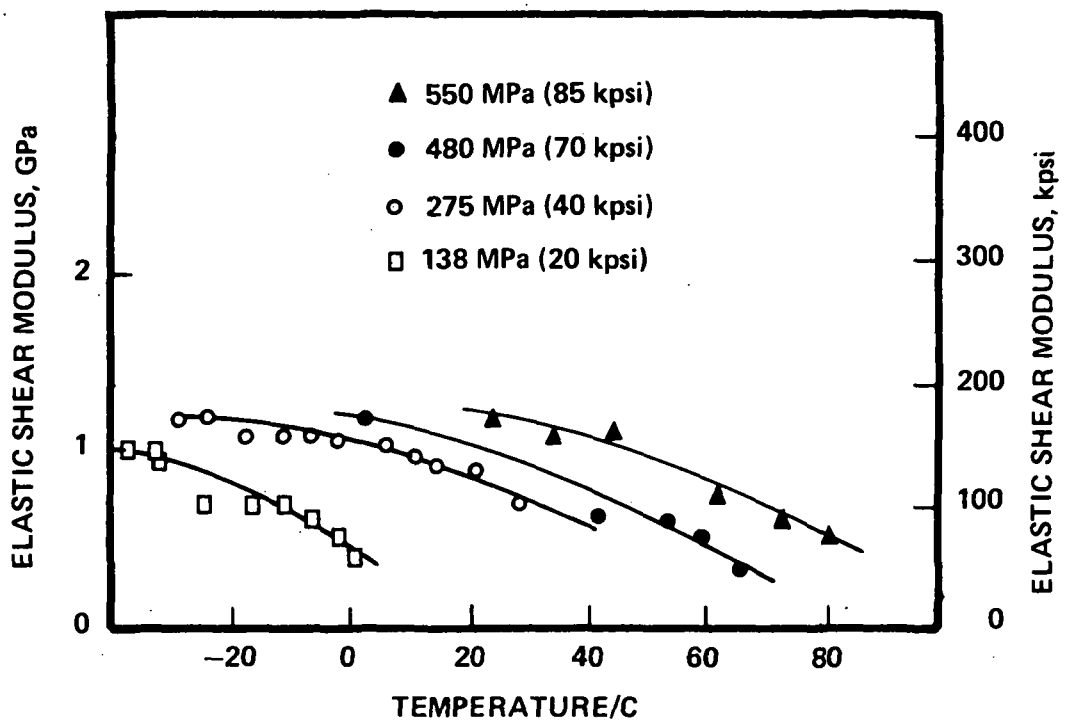

Figure 9. Elastic shear modulus of 5P4E for strain rate of approximately $10^{-2}s^{-1}$

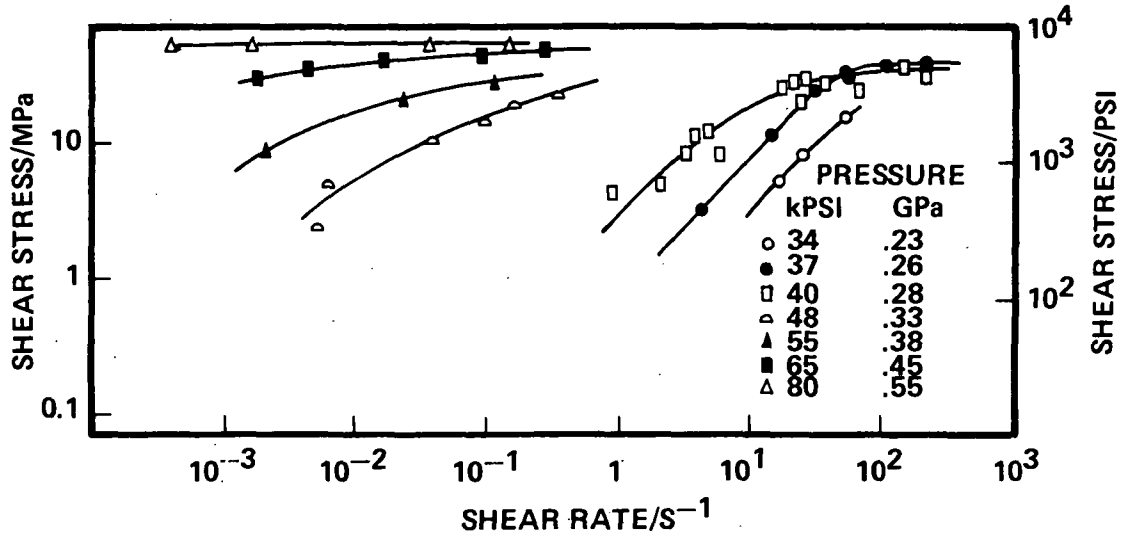

Figure 10. Shear stress-shear strain rate of 5P4E at 40C and indicated pressures

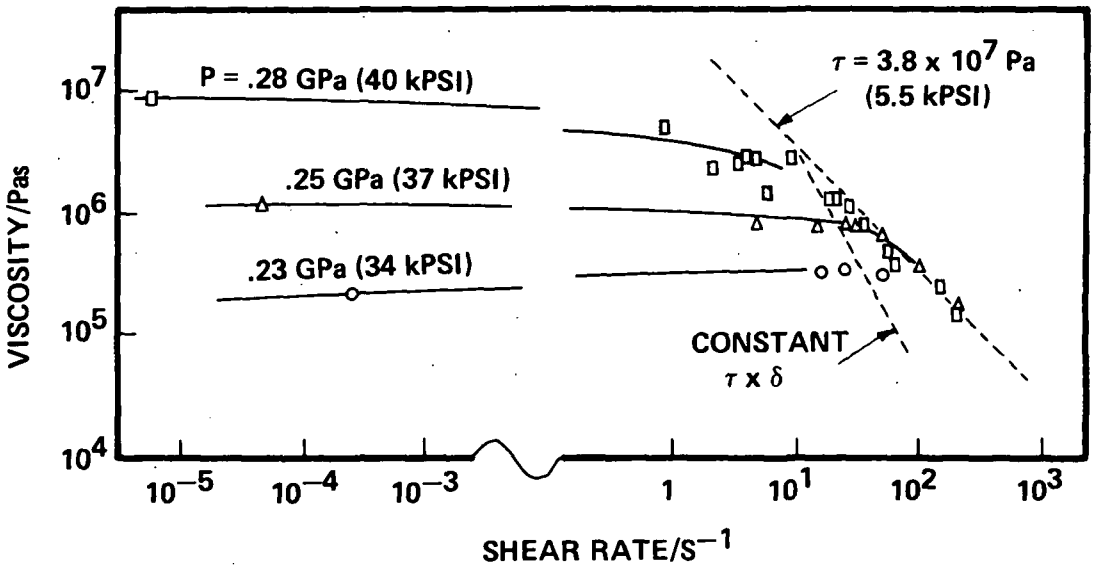

Figure 11a. Viscosity of 5P4E versus shear rate showing the limiting shear stress at 40C

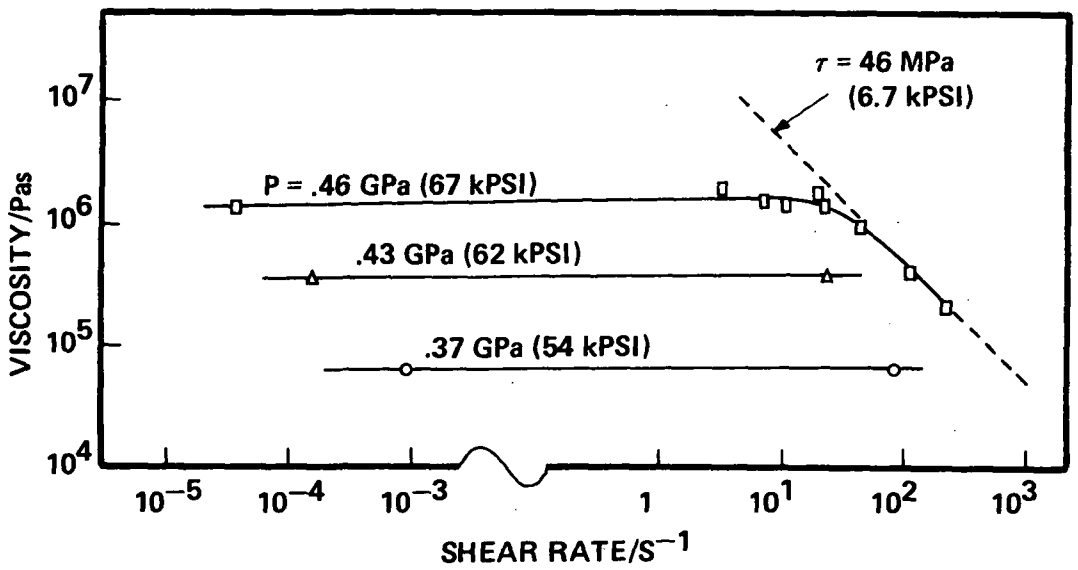

Figure 11b. Viscosity of Santotrac-50 versus shear rate showing limiting shear stress at 20C

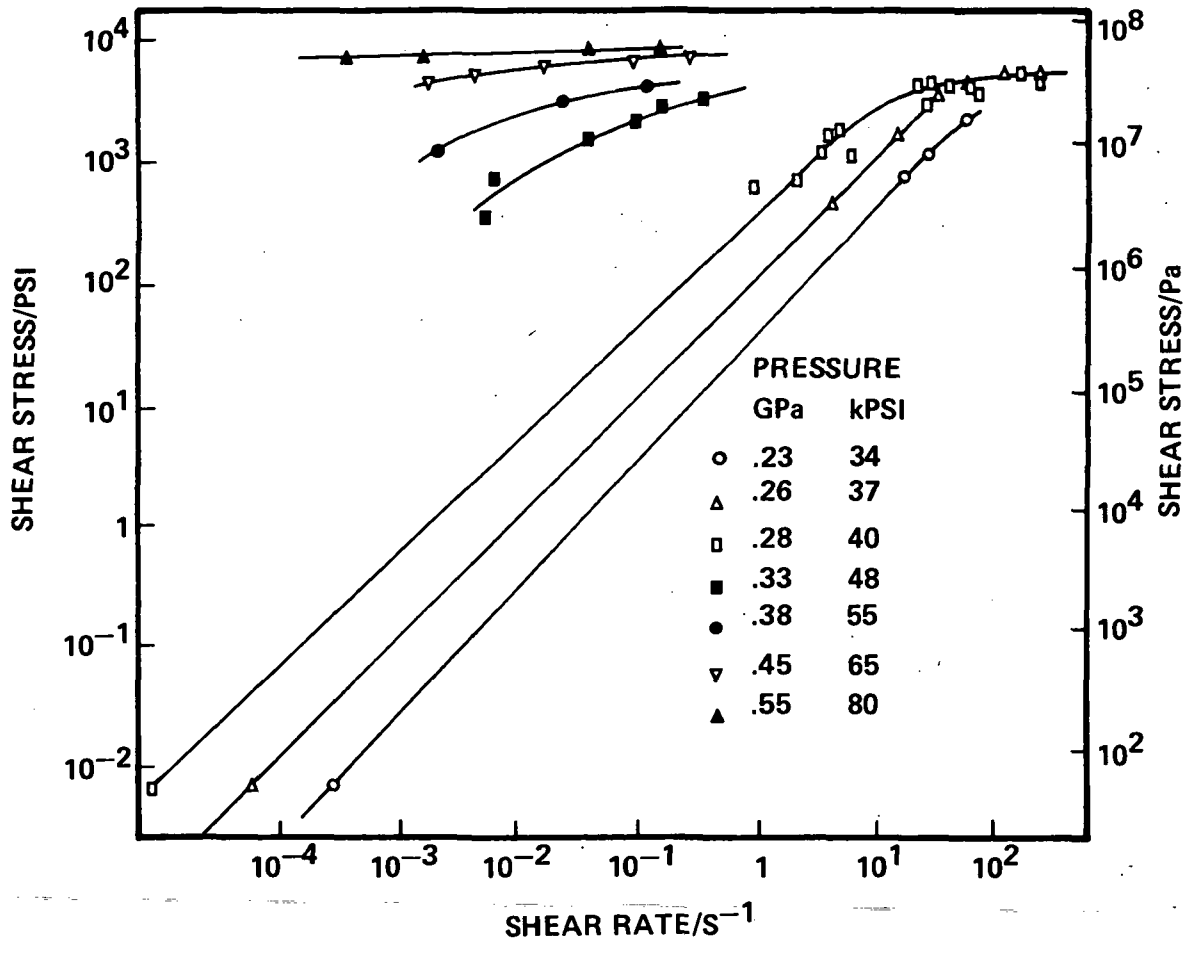

Figure 12a. Shear stress-shear strain rate for 5P4E at 40C and indicated pressure (three different methods-see text)

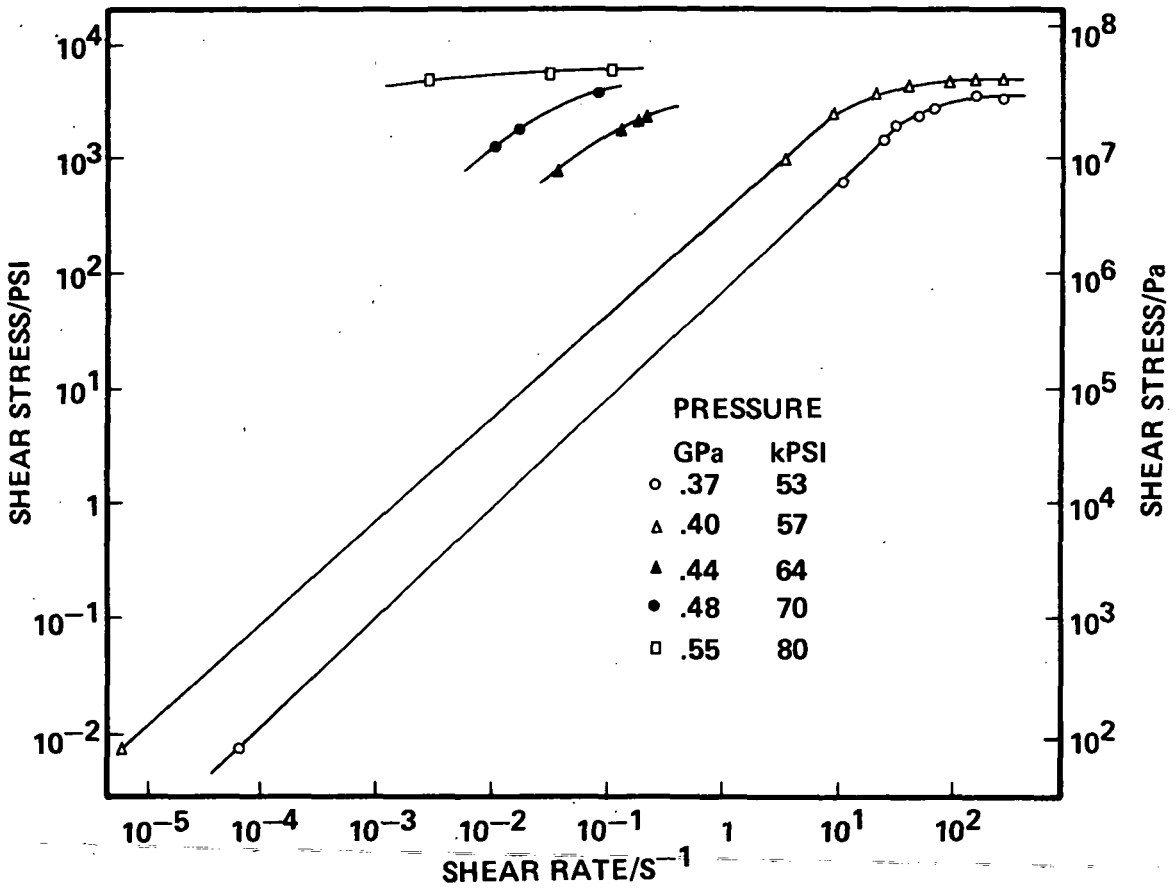

Figure 12b. Shear stress-shear strain rate for 5P4E at 60C and indicated pressure (three different methods-see text)

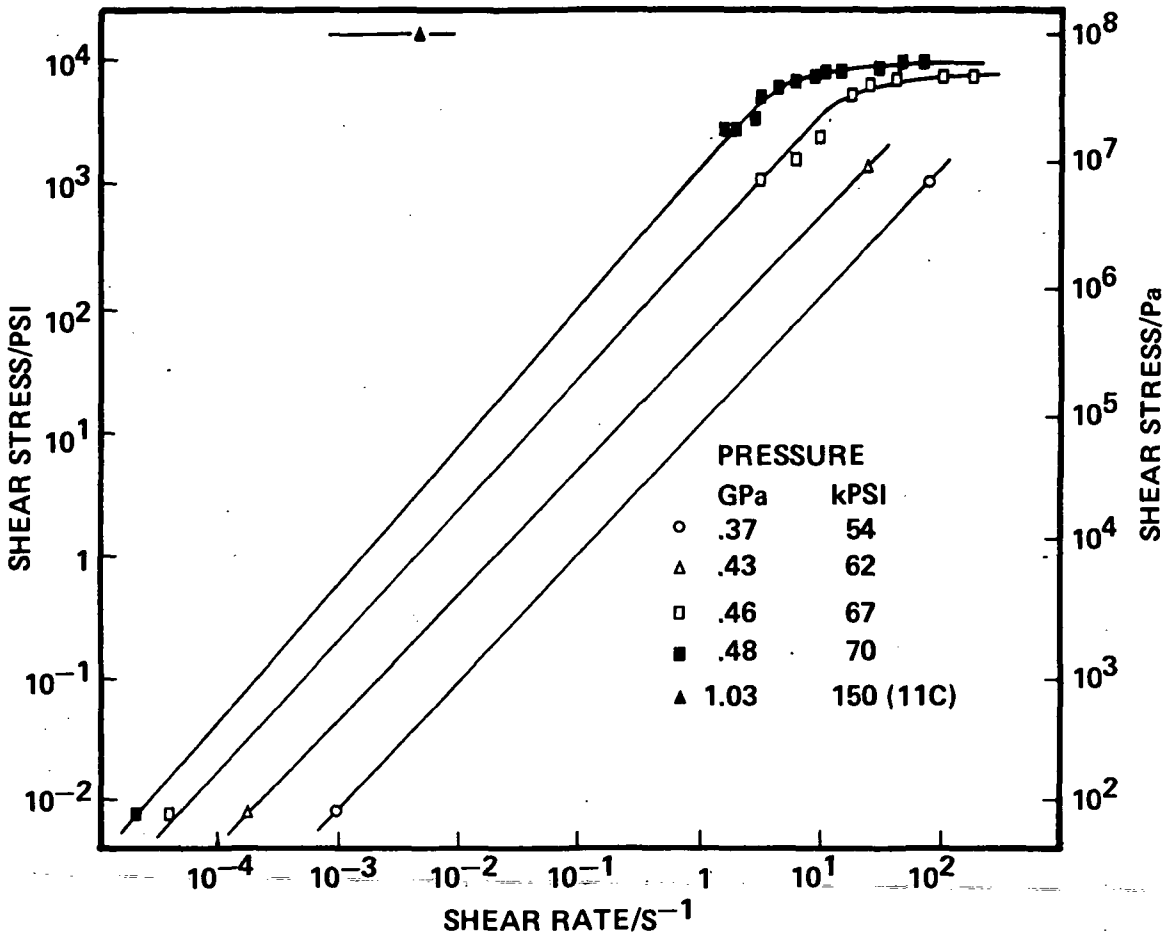

Figure 13. Shear stress-shear strain rate for Santotrac 50 at 20C and indicated pressures (three different methods-see text)

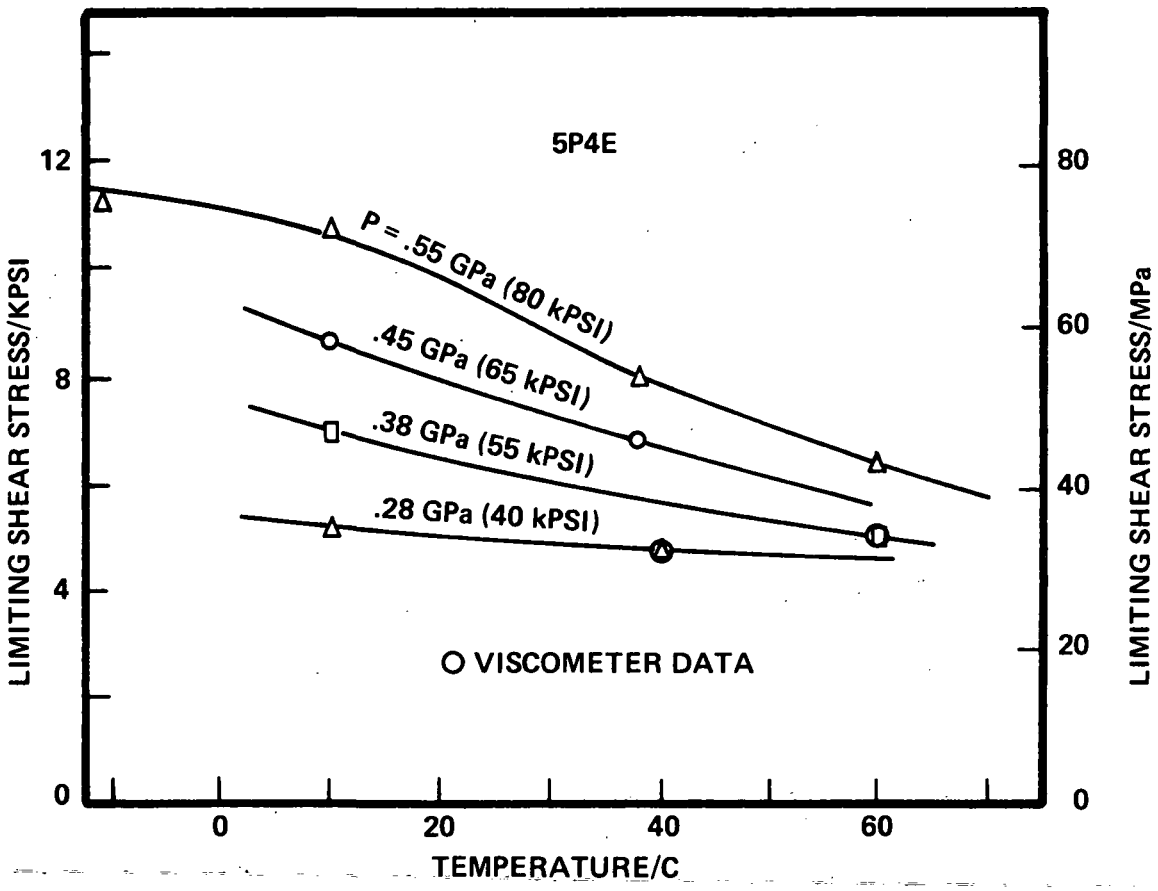

Figure 14a. Limiting shear stress for 5P4E as a function of temperature at indicated pressures. Circle around data point indicates it was obtained with the high stress viscometer (Figure 4)

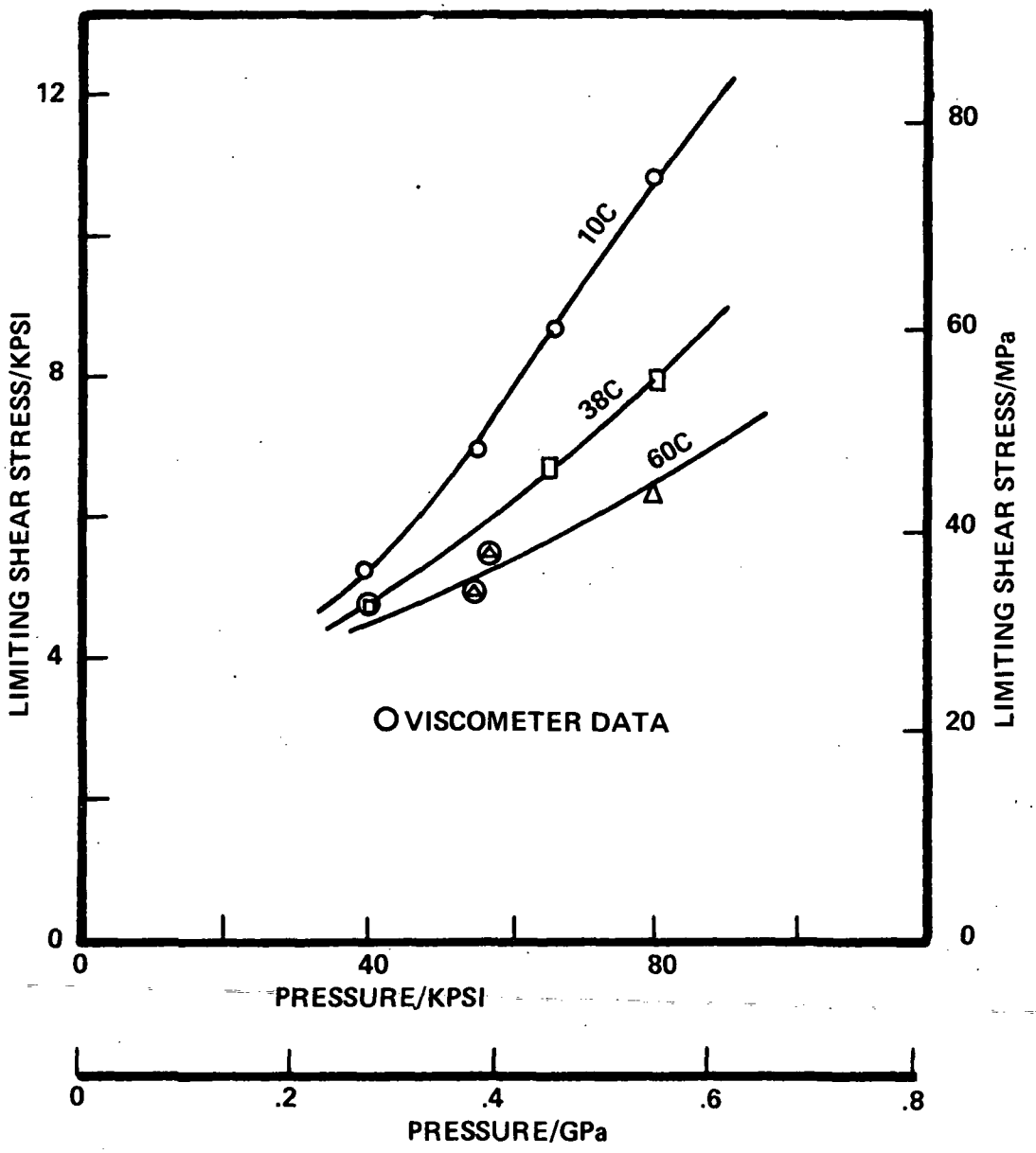

Figure 14b. Limiting shear stress for 5P4E as a function of pressure at indicated temperatures. Circle around data point indicates it was obtained with the high stress viscometer (Figure 4)

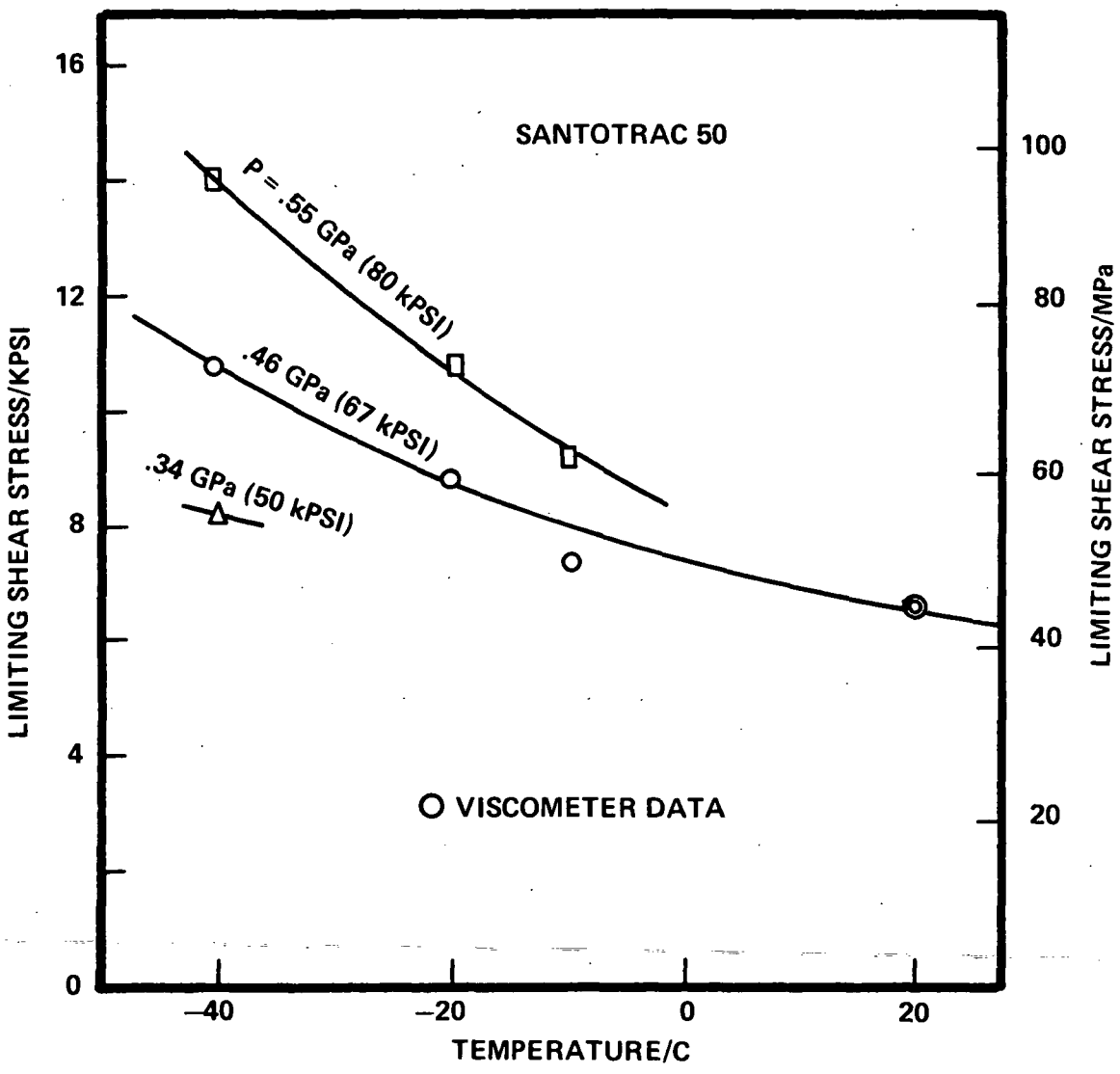

Figure 15a. Limiting shear stress for Santotrac 50 as a function of temperature at indicated pressures. Circle around data point indicates it was obtained with the high stress viscometer

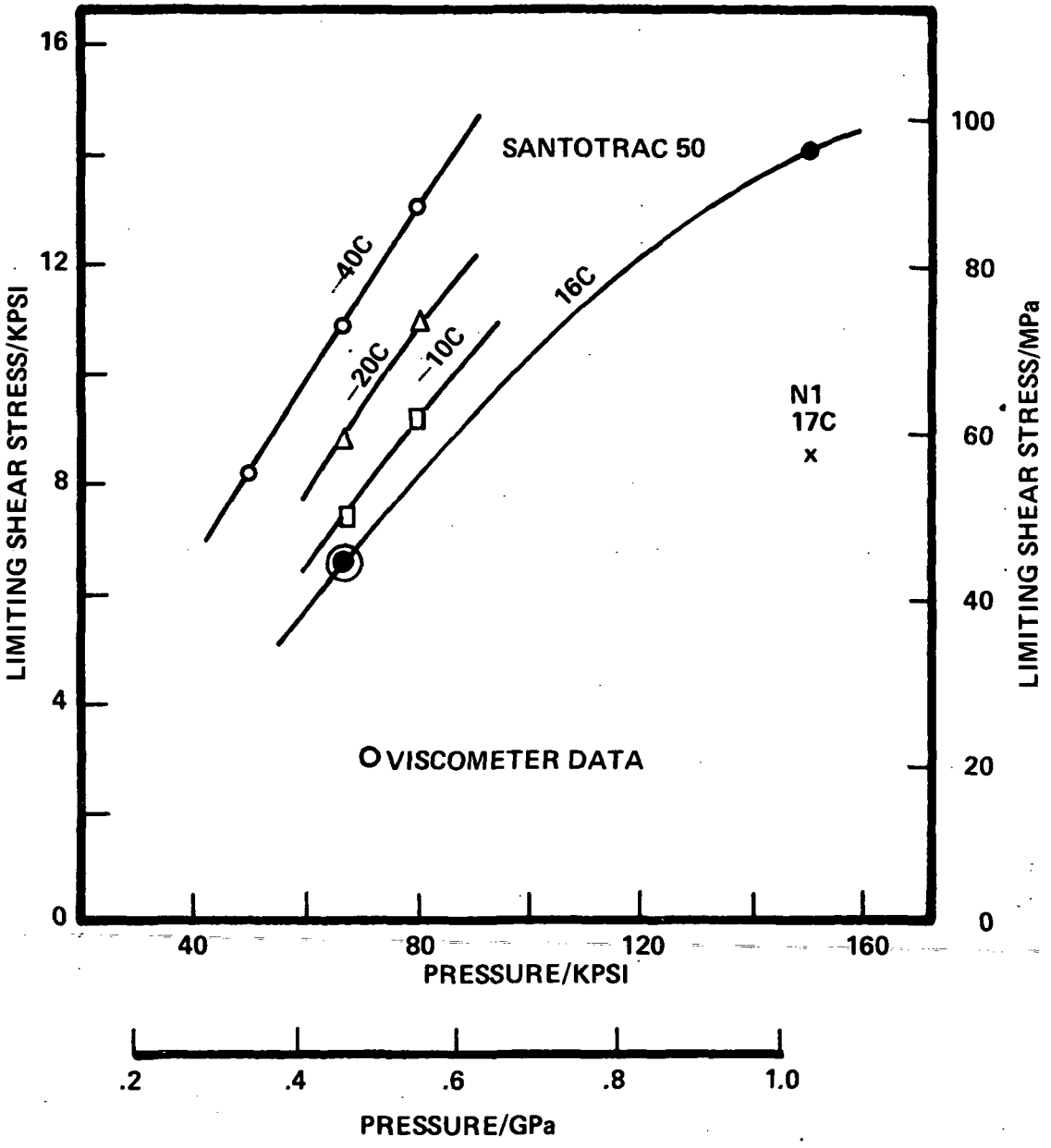

Figure 15b. Limiting shear stress for Santotrac 50 as a function of pressure at indicated temperatures and one data point for N1 is included for comparison

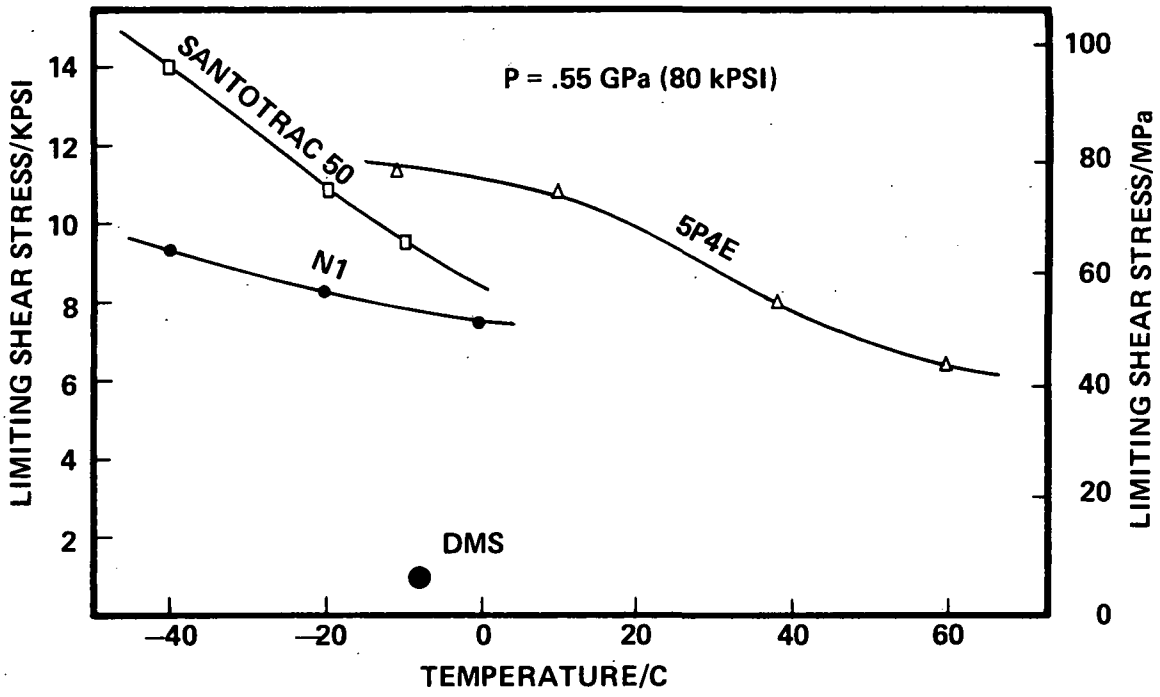

Figure 16. Limiting shear stress for four fluids (N1, Santotrac 50, 5P4E, and dimethylsiloxane (DMS)) at 0.55 GPa

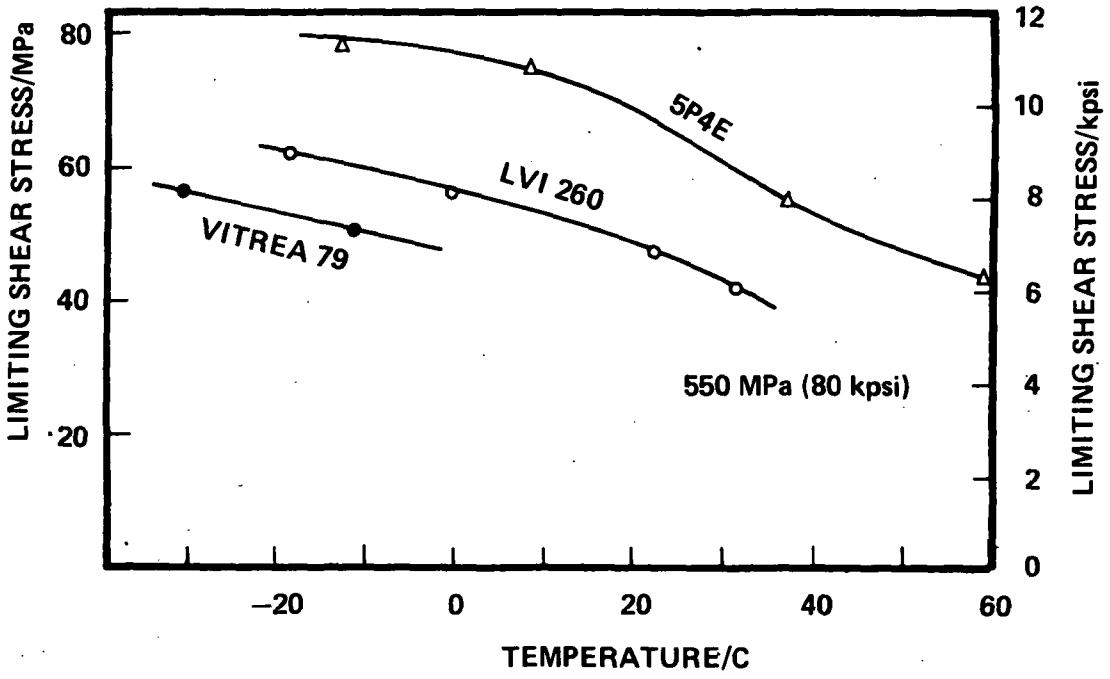

Figure 17. Limiting shear stress at 559 GPa (80 kpsi) for lubricants used by K. L. Johnson et al. in references [6,7]

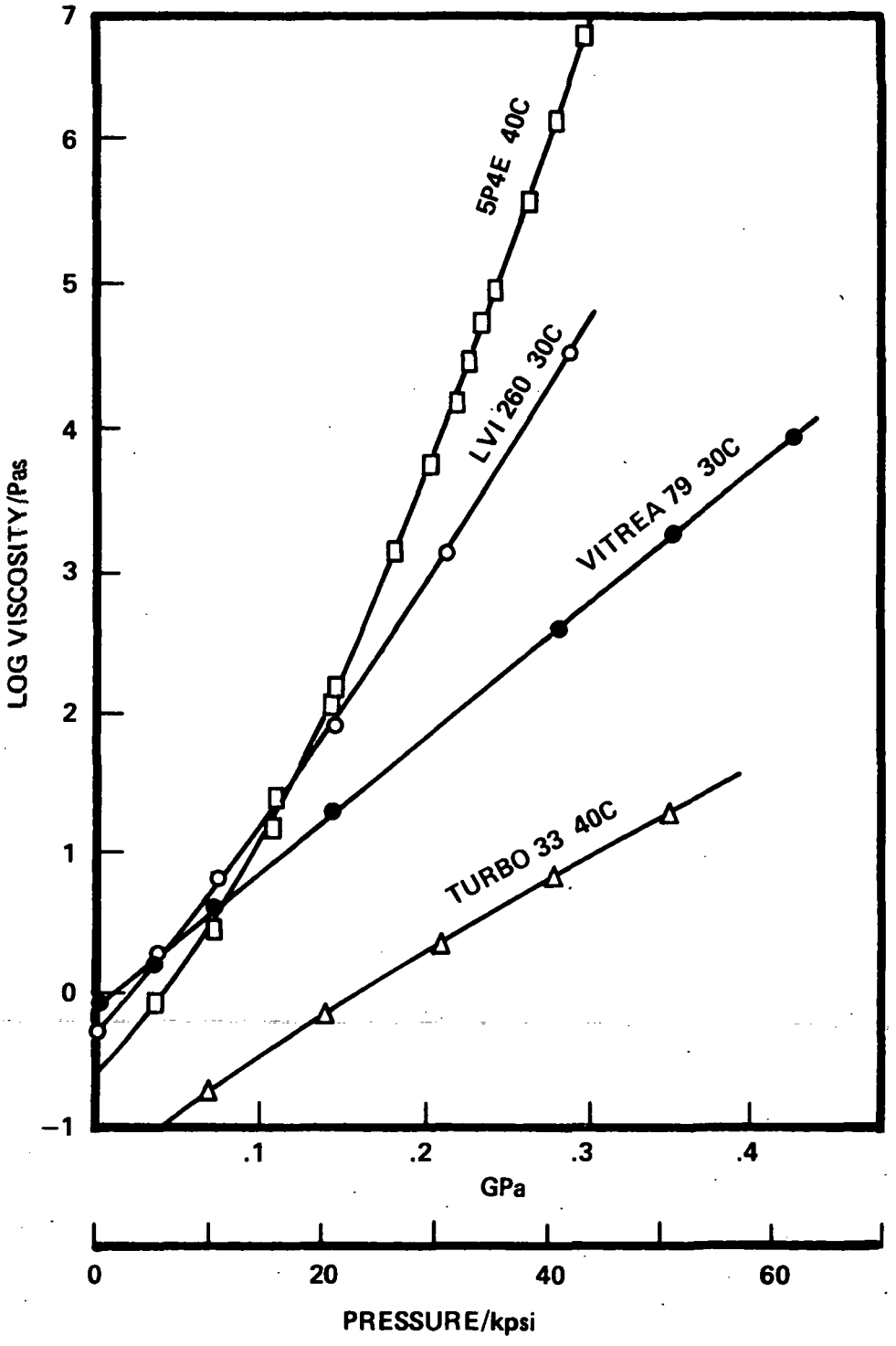

Figure 18. Viscosity-pressure isotherm for lubricants used by K. L. Johnson et al. in references [6,7]

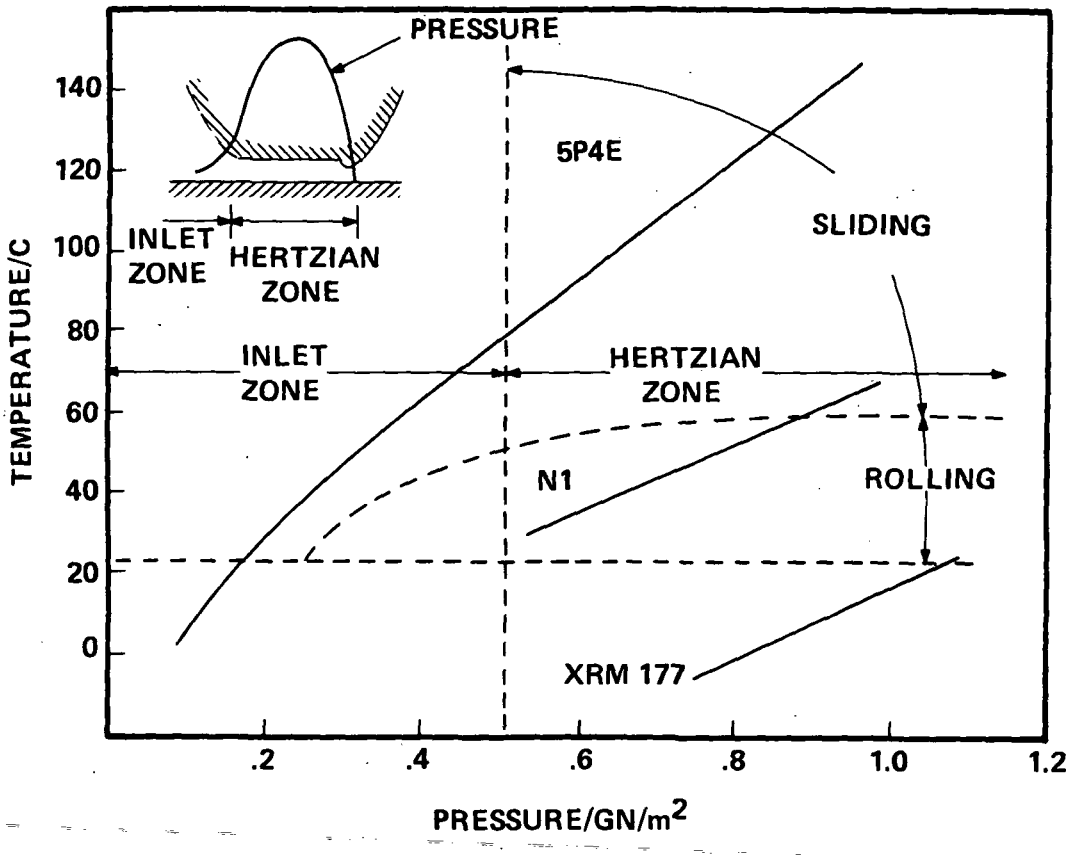

Figure 19. Heuristic estimates of the relationship between conditions in an EHD contact and glass-liquid transition diagram of some lubricants (lubricant supply temperature about 20C)

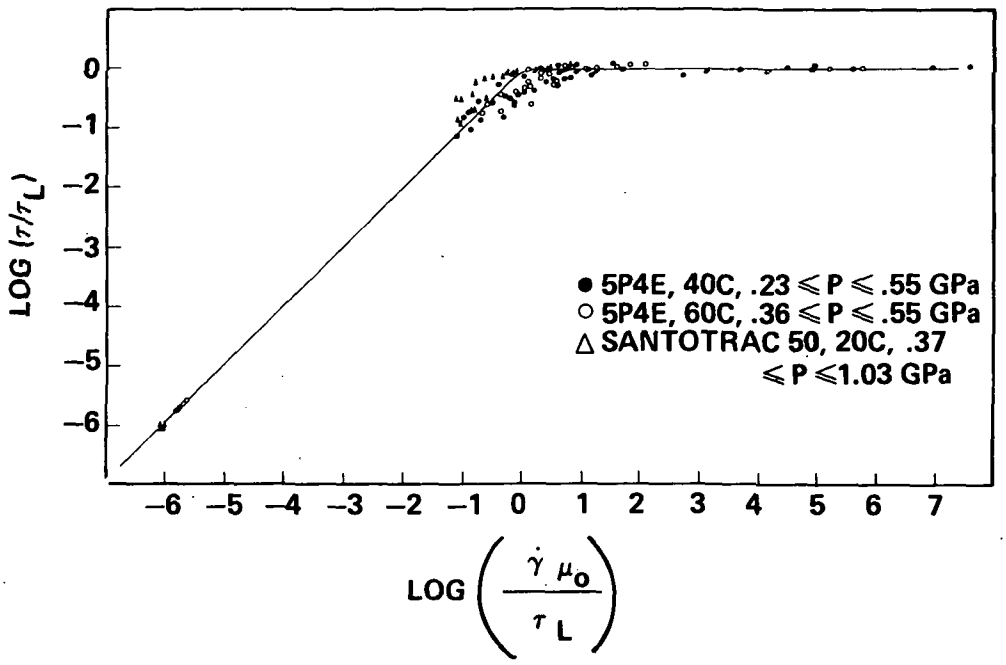

Figure 20. Dimensionless shear stress versus dimensionless shear rate for indicated data

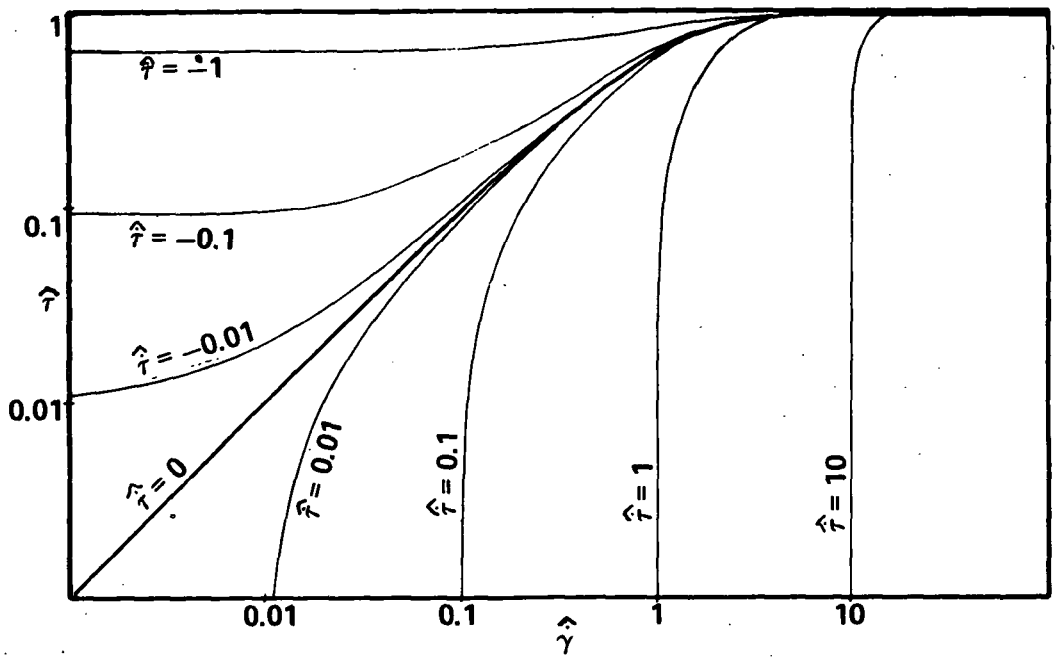

Figure 21. Dimensionless shear stress-shear rate plot from model (Equation 5) for indicated values of dimensionless rate of shear stress application

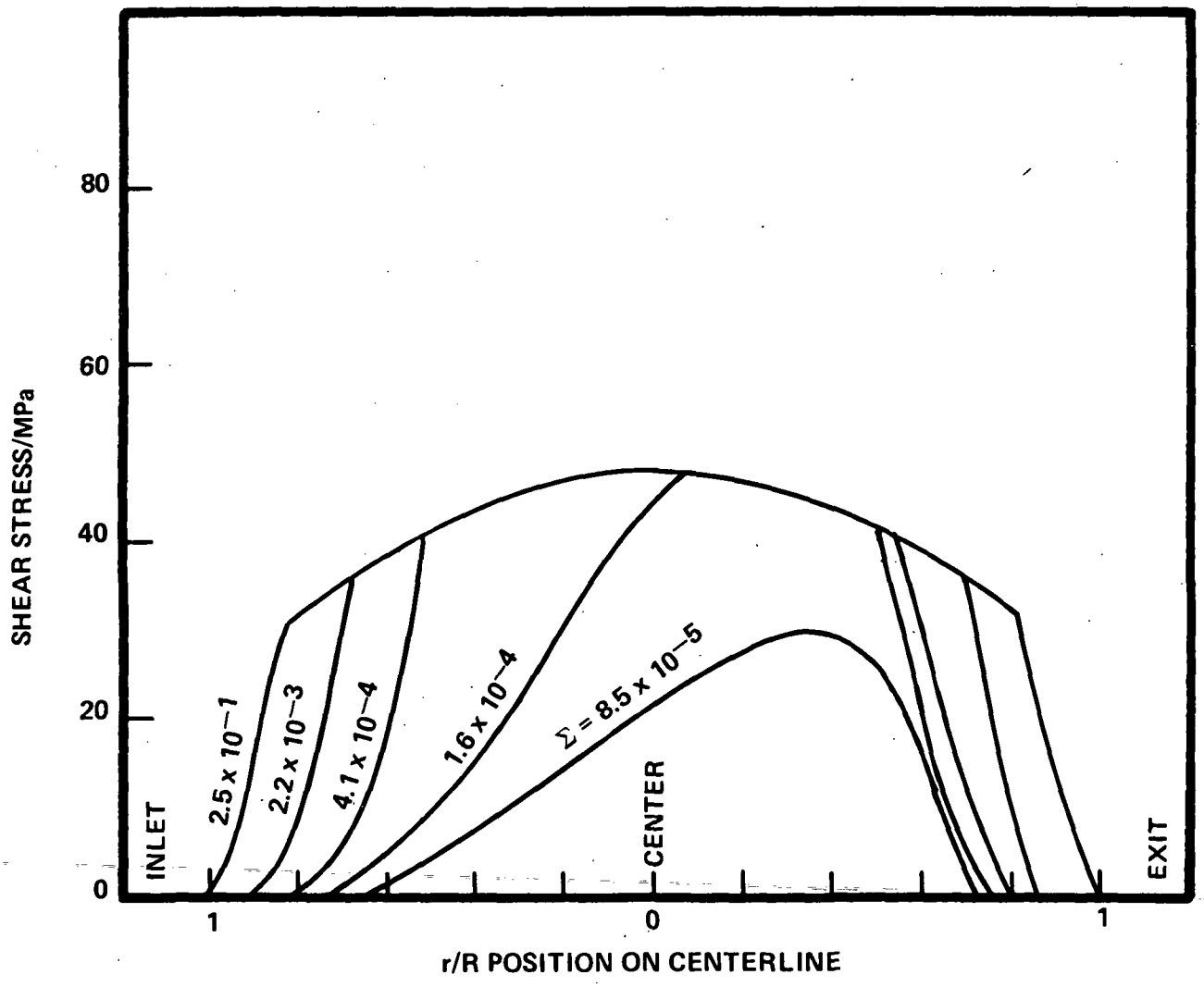

Figure 22. Predicted shear stress distribution in point contact for Santotrac 50 at 20C, 0.5 GPa Hertz pressure, 0.22 m/s rolling speed and indicated slide roll ratios based on equation (5) and measured data

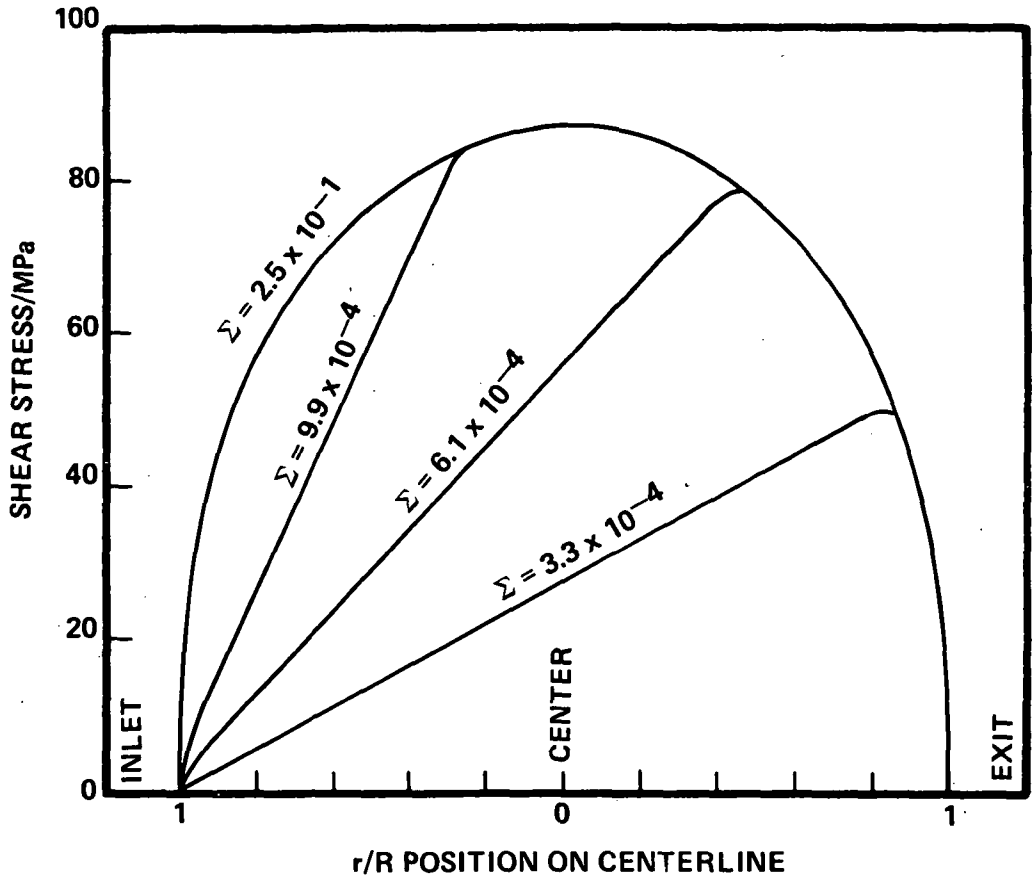

Figure 23. Predicted shear stress distribution in point contact for 5P4E at 40C, 1.0 GPa Hertz pressure, 0.22 m/s rolling speed and indicated slide roll ratios based on equation (5) and measured data

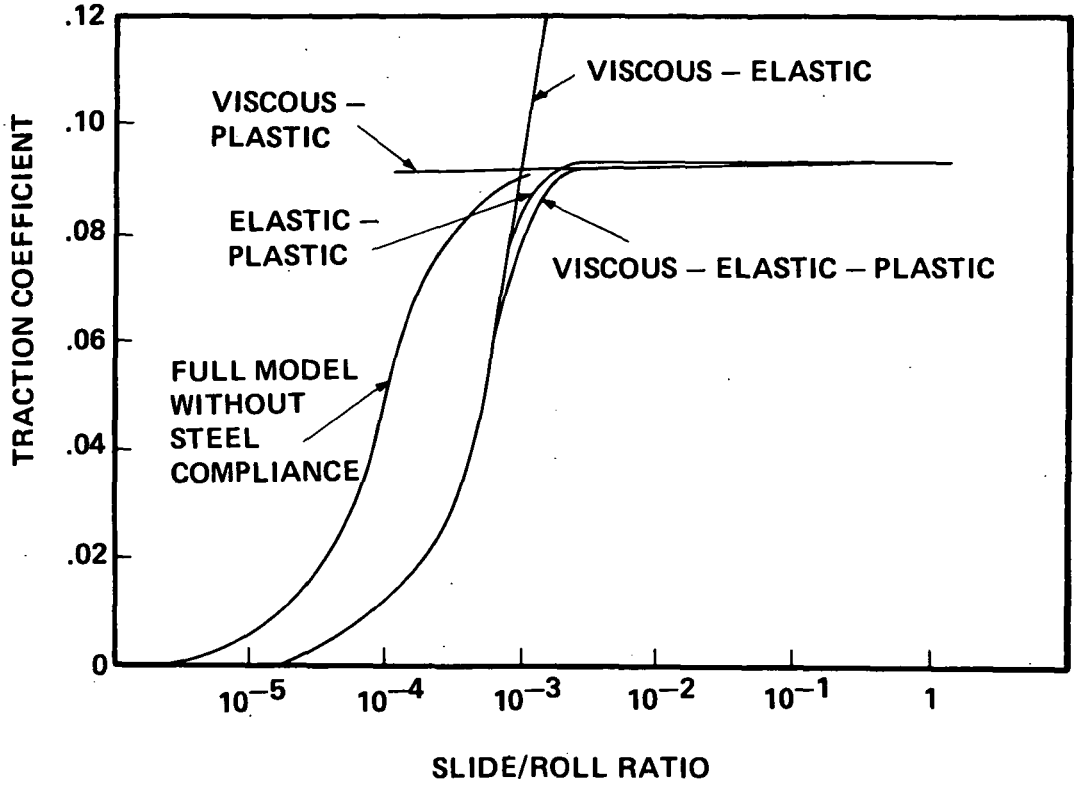

Figure 24. Traction coefficient versus slide-roll ratio for indicated special cases of model (equation 5) for 5P4E, 40C, 1.0 GPa Hertz pressure, and rolling velocity of 0.22 m/s

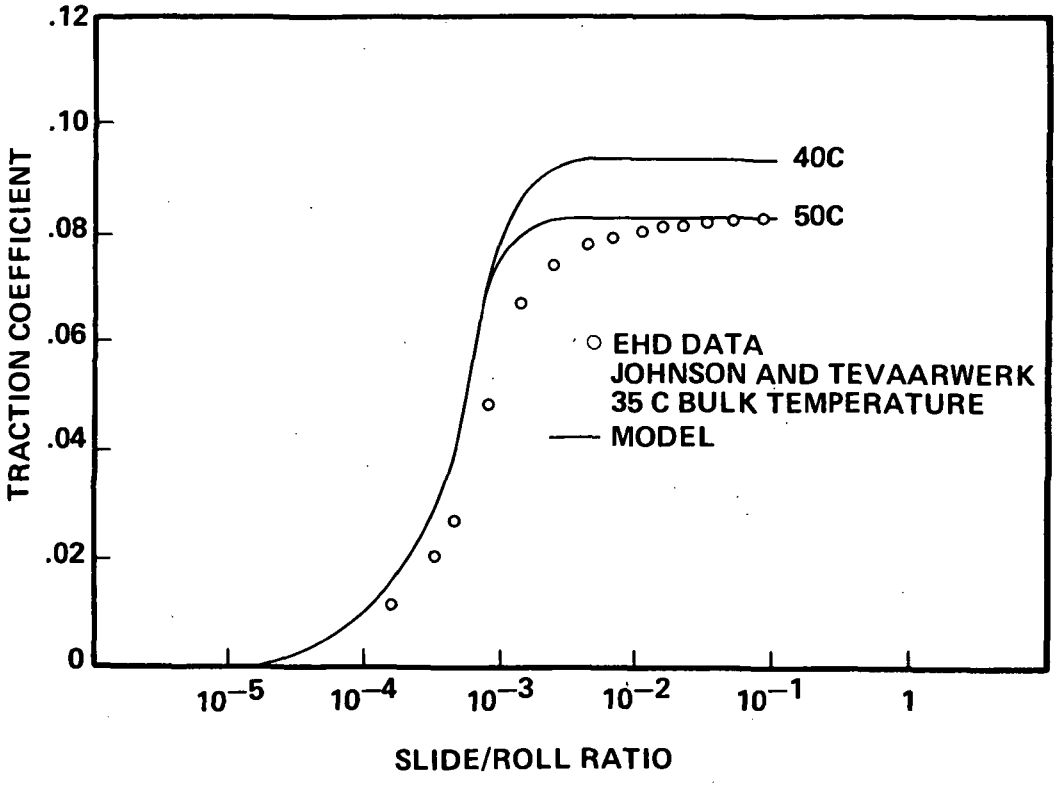

Figure 25. Traction coefficient versus slide-roll for 5P4E, 1.0 GPa Hertz pressure, rolling velocity of 0.22 m/s and indicated temperature. Comparison of model prediction (Equation 5) and measurements of Johnson and Tevaarwerk [20]

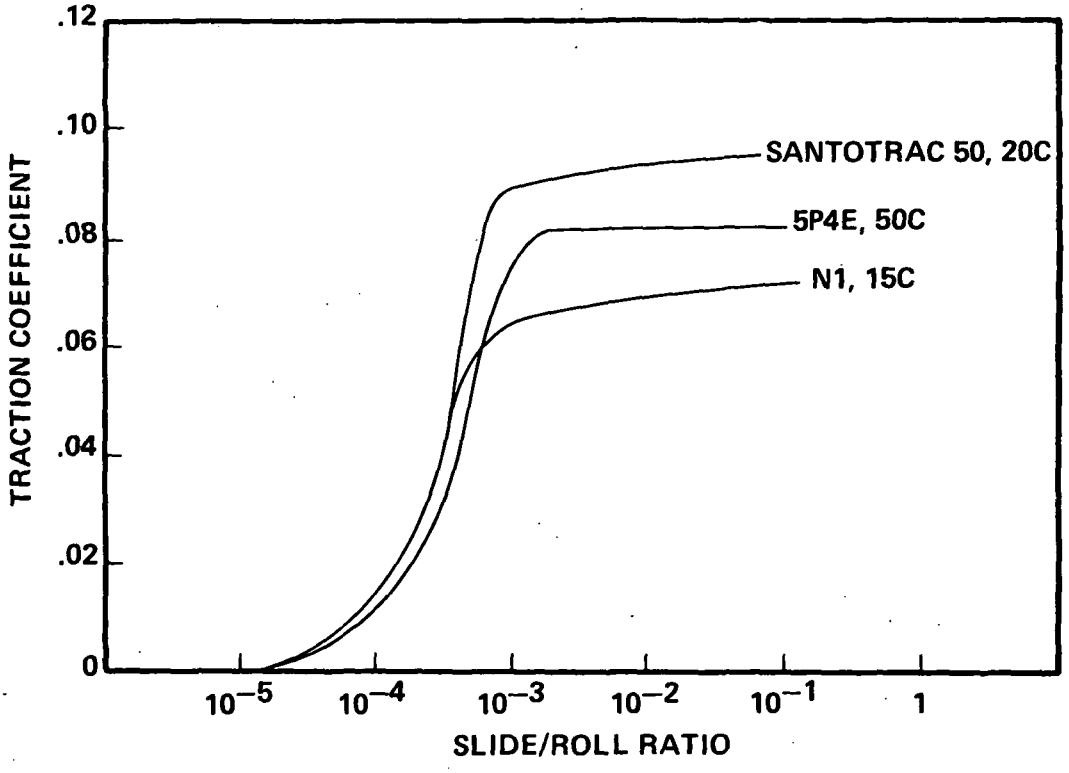

Figure 26. Predicted traction coefficient (Model equation 5 and measured properties) versus slide-roll ratio for indicated lubricants and temperatures at 1.0 GPa Hertz pressure and 0.22 m/s rolling speed

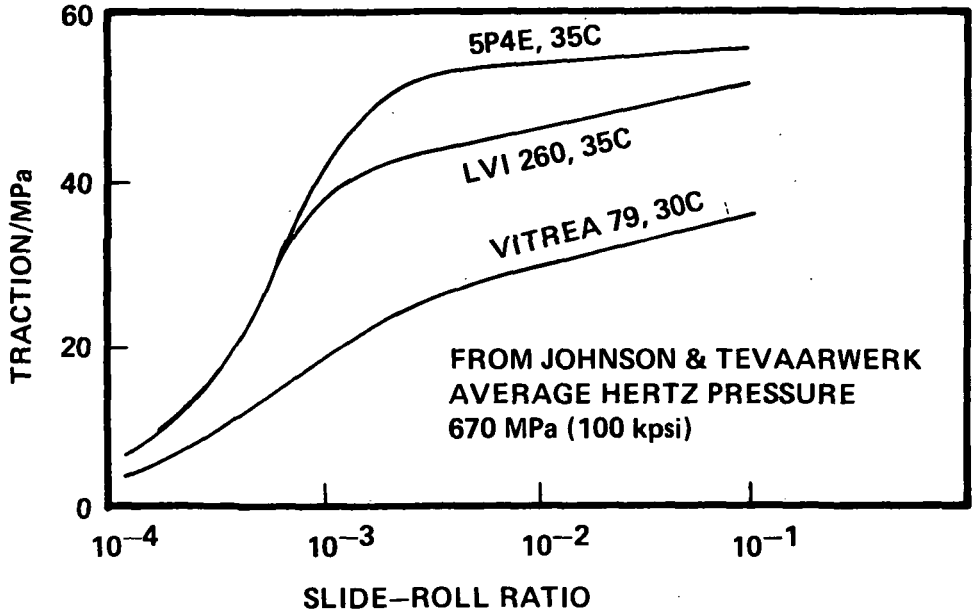

Figure 27a. Measured traction coefficient from Johnson and Tevaarwerk [7]

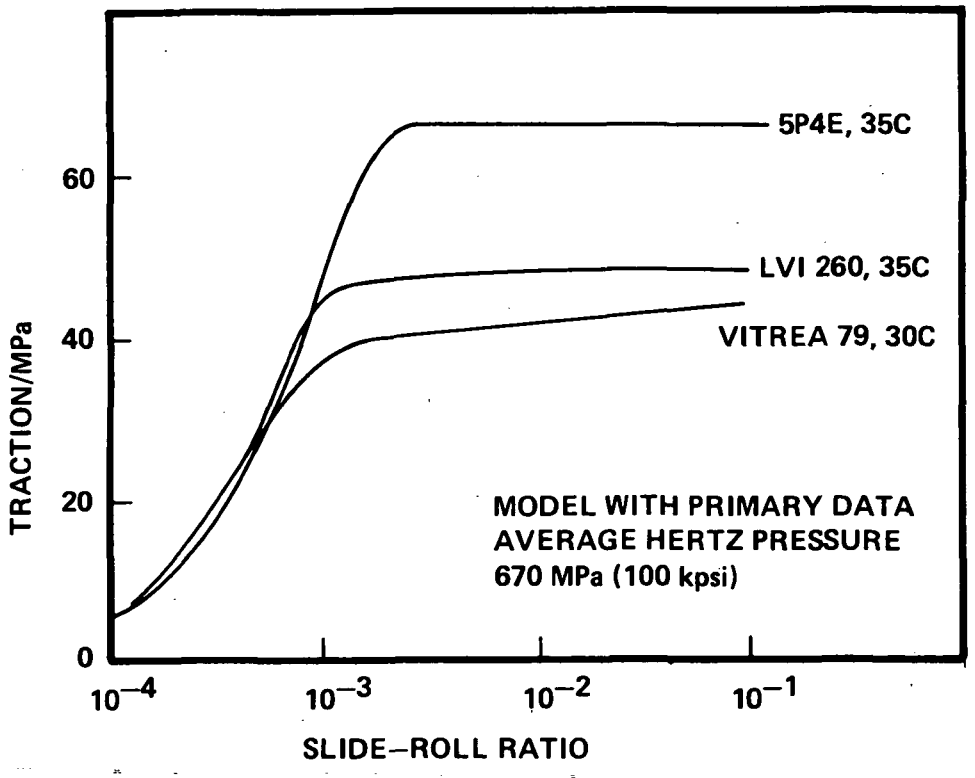

Figure 27b. Predicted traction coefficient for Johnson and Tevaarwerk [6,7] lubricants using model

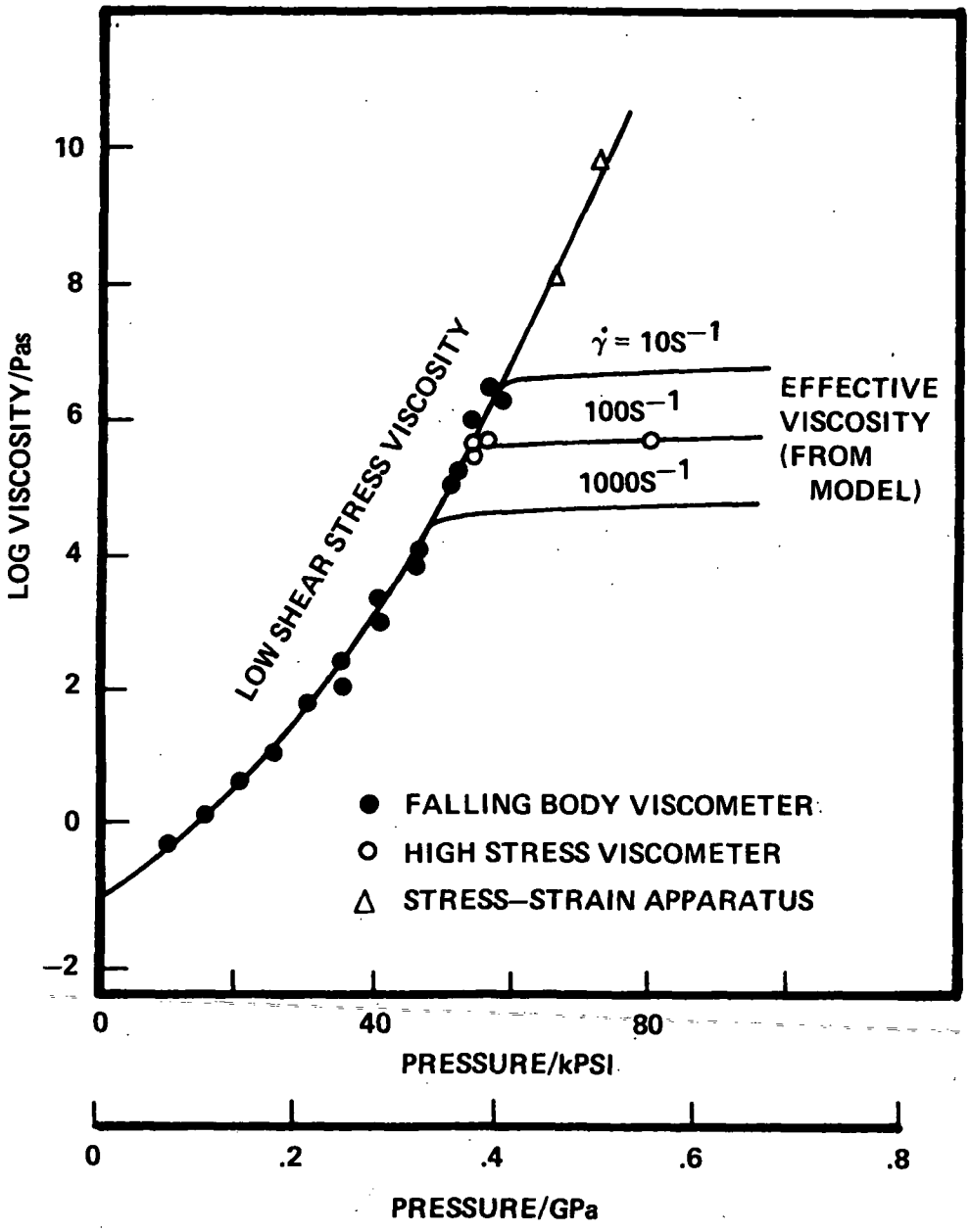

Figure 28. Viscosity pressure isotherm (60C) for 5P4E by indicated methods of measurement. Lines of constant shear rate predicted form model